NACA

RESEARCH MEMORANDUM

AN INVESTIGATION OF THREE TRANSONIC FUSELAGE AIR INLETS AT MACH NUMBERS FROM 0.4 TO 0.94 AND AT A MACH NUMBER OF 1.19

By Robert E. Pendley, Harold L. Robinson, and Claude V. Williams

Langley Aeronautical Laboratory
Langley Air Force Base, Va.

NATIONAL ADVISORY COMMITTEE FOR AERONAUTICS

WASHINGTON
November 7, 1950

NATIONAL ADVISORY COMMITTEE FOR AERONAUTICS

RESEARCH MEMORANDUM

AN INVESTIGATION OF THREE TRANSONIC FUSELAGE AIR INLETS AT MACH NUMBERS FROM 0.4 TO 0.94 AND AT A MACH NUMBER OF 1.19

By Robert E. Pendley, Harold L. Robinson, and Claude V. Williams

SUMMARY

An investigation of three air inlets which were designed for use at transonic speeds was conducted in the Langley 8-foot high-speed tunnel. The basis of the design of these inlets was the use of a nose which was shaped so that substream velocities are maintained on its surface for high-speed operating conditions. Since subsonic velocities would therefore exist on the nose surface up to a limiting supersonic Mach number determined by the nose shape, adverse boundary-layer shock-interaction effects on the nose ahead of the inlet could be avoided at least up to this Mach number.

The three inlets were investigated at an angle of attack of 0° and an angle of yaw of 0° for a Mach number range extending from approximately 0.4 to 0.94 and for a supersonic Mach number of 1.19. The inlet-velocity-ratio range extended from 0 to a maximum value of 1.9. Measurements included external-surface pressure distribution, wake-survey drag, and impact-pressure recovery of the internal flow.

The results of the investigation showed that the maximum values of impact-pressure-recovery coefficient were high (approximately 0.96 at the inlet of configuration A) and were little affected by Mach number over the range investigated. Large external-drag increases were shown for all subsonic Mach numbers when the inlet-velocity ratio was reduced to low values because of either external-flow separation at the inlet lip or increased shock losses. At inlet-velocity ratios in the range of those ratios suitable for high-speed operating conditions, the wake-survey drag coefficient for one of the configurations rose sharply above a Mach number of 0.8. The use of an external shape of higher critical speed in another configuration led to very little increase in the drag up to a Mach number of 0.94 and led also to a substantial reduction in the supersonic external pressure-drag coefficient. The supersonic

pressure drag of this higher-critical-speed configuration was estimated to be approximately equal to that of the NACA 1-40-200 nose inlet and 30 percent greater than that of a closed nose of fineness ratio 6.0.

INTRODUCTION

An investigation of a fuselage-side air inlet designed for use at transonic speeds has been reported in references 1 and 2. The inlet configuration of reference 1 consisted of an NACA 1-series nose inlet (reference 3) of relatively large inlet diameter with a long protruding central body. Three nose or central-body profiles designed to maintain substream velocities over the nose surface under high-speed operating conditions were studied. Since subsonic velocities would exist everywhere on the surface of each of these noses up to a limiting supersonic-flight Mach number determined by the nose shape, adverse boundary-layer - shock-interaction effects on the fuselage nose ahead of the inlet would be avoided at least up to this Mach number. The inlet investigated in reference 2 was the same as one of the inlets of reference 1 except that a pilot's canopy and nose-wheel fairing were added to make a twin side inlet of the basic annular inlet.

The tests of references 1 and 2 were conducted at low speeds. The present paper reports an investigation at transonic speeds of the type of inlet studied in these references. Measurements of external-surface pressure distributions, external skin friction and shock losses, and internal impact-pressure recovery are analyzed.

SYMBOLS

A	stream tube area
C	mass-flow coefficient $\left(\frac{m}{\rho_o F V_o}\right)$
C_{d_s}	wake-survey drag coefficient $\left(\frac{\text{drag}}{q_o F}\right)$
C_{D_p}	external pressure-drag coefficient $\left(\frac{\text{drag}}{q_o F}\right)$
C_{F_c}	central-body pressure-drag coefficient $\left(\frac{\text{drag}}{q_o F}\right)$
D	nose-inlet or cowling maximum diameter
D_p	external pressure drag

F	model reference area $\left(\frac{\pi}{4}D^2\right)$
H	total pressure
m	internal mass-flow rate
M	Mach number
p	static pressure
P	pressure coefficient $\left(\frac{p - p_o}{q_o}\right)$
P_{cr}	critical pressure coefficient, corresponding to local Mach number of 1.0
q	dynamic pressure $\left(\frac{1}{2}\rho V^2\right)$
r	radius, measured from model center line
R	maximum nose-inlet or cowling radius $\left(\frac{D}{2}\right)$
V	velocity
$\frac{V_1}{V_o}$	system inlet-velocity ratio
WL	distance from horizontal plane containing model center line, positive upward
X	longitudinal distance from inlet lip, positive rearward
Y_l	ordinate of inner-lip surface, measured from lip reference line (fig. 1)
Z	lateral distance measured from plane of symmetry
$\left(\frac{H - p_o}{H_o - p_o}\right)_{av}$	average impact-pressure-recovery coefficient $\left(\frac{1}{A}\int_A \left(\frac{H - p_o}{H_o - p_o}\right)dA\right)$
ρ	air density

[redacted]

Subscripts

o	free stream
1	inlet station (minimum duct area just behind inlet lip)
c	central body
d	diffuser rake station
e	inlet rake station (just ahead of minimum area station, see fig. 1)
f	external fuselage surface from inlet to maximum-diameter station
p	pilot's canopy
v	venturi rake station
w	nose-wheel fairing

APPARATUS AND TESTS

Tunnel.- The tests were conducted in the Langley 8-foot high-speed tunnel. The tunnel test section was designed for subsonic test Mach numbers extending up to 0.99 and for a supersonic Mach number of 1.2. The aerodynamic characteristics of the test section are presented in reference 4. For tests at the supersonic Mach number, the central-body apex of each model was located 50 inches downstream of the tunnel effective-minimum-area station; the Mach number in the region of the model was 1.19. For tests at the subsonic Mach numbers, the central-body apex of each model was located 10 inches forward of the tunnel effective-minimum-area station.

Condensation effects at the tunnel test section were avoided by controlling the stagnation temperature by means of the tunnel exhaust and intake vents.

Models.- Three model configurations were investigated. One of the models, designated inlet A, is shown in the upper part of figure 1, and was similar to that investigated at low speeds in reference 2. The same nose inlet or cowling, the NACA 1-85-050, was used. The "short conical nose" of reference 1 was used for the central-body shape, and the canopy lines of reference 2 were used for the external canopy shape. A rounded nose-wheel fairing similar in shape to the canopy was used

pursuant to a recommendation of reference 2. Coordinates for the canopy and nose-wheel fairing are presented in tables I and II.

The other model configurations are shown in the lower part of figure 1. An NACA 1-80-100 nose inlet was fitted with two interchangeable central bodies. The conical central body was identical with the central body of inlet A, and the profile of the curved central body (shown as a dashed line) was taken from reference 1. Central-body coordinates are given in table III. When equipped with the conical central body this inlet is designated inlet B, and with the curved central body, inlet C. These inlets were investigated only as annular inlets. The maximum diameter of both NACA 1-series nose inlets was 3 inches.

Inlet B was designed for the purpose of investigating the effect of using a higher-critical-speed external surface rearward of the inlet lip. As stated in reference 1, the curved central-body profile of inlet C was designed for increased volume within the nose.

The NACA 1-series nose inlets used as the basic components of the inlets utilized inner-lip nose radii 1.5 times normal after a suggestion of reference 3. Coordinates of the inner-lip fairing are given in figure 1, and the external-cowling ordinates may be obtained from reference 3.

Model mounting.- The models were mounted on a sting which was supported along the tunnel axis (fig. 2). Bearings in the sting supports permitted longitudinal motion of the sting so that the model could be conveniently positioned in either the subsonic or supersonic test section. Three guy wires (fig. 2) were used to rigidly fix the models at an angle of attack of 0° and a yaw angle of 0°.

Connecting members between the inlet models and sting are shown in figure 3. The models were mounted on a length of straight pipe of 3-inch outside diameter; this pipe was attached to a tapered pipe which was terminated at the exit of the internal-flow duct.

Internal-flow ducting and instrumentation.- Internal-flow rate was regulated by controlling the exit area by means of the sliding ball shown in figure 3. The internal flow was diffused from the inlet to the straight pipe, then expanded through a venturi, and finally diffused to the exit. The length of straight pipe between the inlet and venturi was provided to reduce the rotational variations of the flow at the venturi. Angular surveys at the venturi showed that the flow there was closely axially symmetric so that it was possible to use a single diametrical survey rake of total-pressure and static-pressure tubes for measuring the mass flow.

[redacted]

Survey rakes of total-pressure tubes were used to measure impact-pressure recovery in the internal-flow ducts. Inlet A was equipped with a rake near the inlet of the right duct and one in the diffuser of the left duct. The locations of these rakes are shown in figure 1. The diffuser rake was located at that point in the diffuser where the duct area was 2.31 times the inlet area. This rake was constructed of tubes with 0.020-inch outside diameter and 0.010-inch inside diameter. The inlet rake was made of 0.040-inch-diameter tubing, the ends of which were flattened to form openings about 0.005 by 0.045 inch. The tubes of this rake were led out through the external-model surface and downstream in a flat belt normal to the surface.

Inlets B and C were equipped with a total-pressure rake located 1.29 inches downstream of the inlet lip, where the duct area was approximately 30 percent greater than the inlet area. This rake was constructed and mounted like the inlet rake of inlet A.

External pressure orifices and wake-survey rake.- For each inlet, pressure distribution was measured on the external surface rearward of the inlet by a single longitudinal row of pressure orifices, and on inlet A a single pressure orifice was located on the central body 0.3 inch ahead of the inlet. The locations of these orifices are shown in figure 1.

An external survey rake of total-pressure and static-pressure tubes was used to measure external boundary layer and shock losses at subsonic Mach numbers. The position of this rake is shown in figure 3. The first eight inboard tubes of the rake had an outside diameter of 0.030 inch and were assembled in a solid band with the first tube in contact with the model surface. The other tubes of the rake had an outside diameter of 0.050 inch. Static-pressure tubes were offset about 0.3 inch from the plane of the total-pressure tubes.

Tests.- Data were recorded by photographing multitube manometers for a range of free-stream subsonic Mach numbers extending from approximately 0.4 to 0.94 and for the supersonic Mach number of 1.19. The corresponding Reynolds number range, based on the cowling maximum diameter, extended from approximately 6.1×10^5 to 9.8×10^5. The inlet-velocity ratio was varied from 0 to a maximum value of 1.9.

Measurements at the Mach numbers of 0.9 and 1.19 were made both without and with artificial transition strips applied to the central body and external cowling surface of inlet A. These strips were 3/16 inch wide and were made of No. 60 carborundum grains cemented to the surface. The trailing edge of the circumferential strip on the nose was about 1.5 inches forward of the inlet. The strip on the external cowling surface was placed with its leading edge at the inlet lip and was not applied to the canopy or nose-wheel fairing surfaces.

[redacted]

METHODS AND PRECISION

Tunnel-wall corrections.- Because of the small size of the model relative to the tunnel test-section dimensions, no wind-tunnel-wall corrections have been applied to the data.

Inlet-velocity ratio.- The values of inlet-velocity ratio given in this paper were calculated from the internal mass-flow rate and the inlet area. (See reference 5.) Isentropic flow was assumed from the free stream to the inlet for subsonic Mach numbers; and for the supersonic Mach number, an inlet total-pressure decrement equal to the total-pressure loss through a normal shock from the free-stream Mach number was assumed. These values of inlet-velocity ratio are thus of a nominal nature because of the presence of boundary layers and velocity gradients at the inlet. A chart is provided in figure 4 for convenient conversion from inlet-velocity ratio to either the mass-flow coefficient A_o/A_1, which is based on the inlet area, or the mass-flow coefficient C, which is based on the reference area F.

The precision of the inlet-velocity-ratio calculations was influenced by the free-stream Mach number, the internal-flow rate, and the inlet area. The largest errors for inlet-velocity ratios of 0.1 and 0.6 were approximately ±0.05 and ±0.02, respectively. The maximum error in inlet-velocity ratio grew smaller as the inlet-velocity ratio was increased above 0.6 until, for the free-stream Mach number involved, choking at the inlet was approached. At that point the maximum error was amplified to approximately ±0.03 as a result of the rapid rate of change of inlet-velocity ratio with mass-flow coefficient near inlet-choked conditions. The error in mass-flow coefficient always regularly decreased with increasing flow rate.

The inlet-velocity ratio at which the data indicate that the inlet was choked in some cases was substantially less (by approximately 0.13 in one instance) than the one-dimensional value which can be calculated from the ratio of the inlet to the free-stream Mach number for an inlet Mach number of unity. Part of this discrepancy may be ascribed to the error mentioned above, and the remainder was probably due to the effective reduction of the minimum duct areas by boundary layers.

Impact-pressure recovery.- At any given inlet-velocity ratio above that for boundary-layer separation from the central body ahead of the inlet, the presence of the pilot's canopy and the nose-wheel fairing of inlet A probably exerted little influence on the total-pressure recovery at the locations of the pressure-recovery rakes. If this assumption is true, the measurements are equivalent to those that would be obtained for the inlet in its annular form.

[redacted]

The impact-pressure recovery was weighted against area rather than against the local mass flow in the integration used to compute the average pressure-recovery coefficient (see symbols) since no static pressures in the ducts were measured. Larger values would result if the pressure recoveries were weighted against mass flow. The increment between the values given by the two methods would be largest for those cases where extensive total-pressure gradients existed across the duct but would be negligible for those cases where the total-pressure distribution was flat across almost the entire duct. The maximum increment in impact-pressure-reoovery coefficient that would be obtained by weighting against mass flow rather than against area would occur in the case of the diffuser survey of inlet A and is estimated to be of the order of +0.05.

External measurements.- As in the case of the pressure-recovery measurements, the presence of the pilot's canopy and nose-wheel fairing of inlet A is not believed to have had a large effect on the external-surface pressure distribution and the losses measured by the external survey rake. The external pressure drag and wake-survey drag coefficients were computed by neglecting the presence of the canopy and nose-wheel fairing; in other words, the measurements of pressure distribution obtained in one radial plane were treated as measurements in an axially symmetrical flow field. The validity of comparing the measurements of inlet A with those of the annular inlets B and C is thus dependent on the amount of canopy and nose-wheel-fairing interference.

The data obtained at the subsonic Mach numbers with the external survey rake were computed by the usual method of computing drag from a wake survey (reference 6). The values of the drag coefficients obtained in this manner from the wake survey of the present investigation are useful in evaluating changes in the forebody drag which result from changes in the inlet-velocity ratio, Mach number, or model shape.

External pressure drag.- The external pressure-drag coefficient has been calculated from the pressure distributions measured at the supersonic test Mach number by a method complementary to that of reference 7. The basis of the method can be visualized by consideration of a hypothetical inlet-afterbody combination. For annular inlets, the central body is assumed to be cylindrical between the inlet and an annular exit, the area of which is calculated to obtain free-stream pressure at this point. Behind the exit, the central body is assumed to taper so gradually that the pressure acting on its surface is equal to the free-stream pressure, and the exterior surface of the inlet downstream of the maximum-diameter station is also assumed to taper so gradually that free-stream pressure acts on this surface. The external pressure drag is then defined as the sum of the dragwise components of all pressure forces acting internally and externally minus the internal drag resulting from the momentum defect of the jet. This momentum defect is assumed to arise only from the total-pressure loss of a normal shock from the free-stream Mach number (internal

[redacted]

flow assumed isentropic downstream of the normal shock). Negligible differences would result if this momentum defect had been calculated from the total-pressure loss through the actual shock configuration because of the low supersonic free-stream Mach number. When calculated by the above method, the external pressure drag reduces to the following expression

$$D_p = \pi \int_{(r_1^2)}^{(R^2)} p_f \, d(r^2) + \pi \int_{o}^{(r_c^2)} p_c \, d(r^2) + m(V_1 - V_o) - p_o F + p_1 A_1$$

The foregoing method neglects the effects of the central-body boundary layer on the external-pressure forces. These effects are expected to be negligible for conditions of unseparated central-body flow ahead of the inlet.

The scarcity of pressure orifices in the vicinity of the leading edge of the inlet lip led to an estimated precision in the external pressure-drag coefficient of ±0.02.

RESULTS AND DISCUSSION

Impact Pressure Recovery

Representative impact-pressure-recovery distributions are presented in figures 5 and 6, and the variation of the average-impact-pressure-recovery coefficient with inlet-velocity ratio is presented in figures 7 and 8. Because of twin-duct flow instability which is discussed in the following section, the individual inlet-velocity ratios of the two branches of the duct of inlet A are not known below system inlet-velocity ratios of approximately 0.6; hence, all curves for inlet A are dashed curves below this value of system inlet-velocity ratio.

Inlet A.- At the lower system inlet-velocity ratios the central-body boundary layer of inlet A was relatively thick because of the adverse pressure gradient acting ahead of the inlet (fig. 5(a)). As the inlet-velocity ratio was increased this gradient was reduced and the central-body boundary layer became thinner. An impact pressure closely approaching that of the free stream was available over much of the inlet at the higher inlet-velocity ratios at all Mach numbers including the supersonic Mach number of 1.19. At the Mach number of 1.19 full free-stream impact pressure was not obtained in any point in the inlet because of small total-pressure losses through shocks on the central body.

Visual observation of the shock pattern on the central bodies with the aid of a concentrated arc lamp showed an attached shock at the apex of the central body and, since the test Mach number was greater than

the minimum for supersonic flow on the surface, a normal shock, which was estimated to be about one inch ahead of the inlet, existed on the central body. This normal shock curved gradually rearward and, at the limits of the field of view, appeared to be approaching the shock which was attached at the apex of the central body. As a result of the pressure rise associated with the normal shock, the central-body boundary layer at the inlet was thicker for the supersonic Mach number than for any of the subsonic Mach numbers.

Average pressure recoveries for inlet A measured at the entrance of one branch of the intake duct and in the diffuser of the other branch of the duct at longitudinal station 3.05 where the area was 2.31 times the inlet area are presented in figure 7. The maximum values of pressure recovery were high and were little affected by Mach number over the range investigated.

Some of the curves of figure 7 show a rapid decrease in pressure recovery at inlet-velocity ratios of 0.4 to 0.6 as the inlet-velocity ratio was decreased from the higher values. These decreases were caused by boundary-layer separation from the central body ahead of the inlet and would be expected to occur at inlet-velocity ratios of this order. Other curves, however, indicate high pressure recovery at very low inlet-velocity ratios. Also, at the lower inlet-velocity ratios, the pressure recovery measured in the diffuser of one branch of the duct sometimes was higher than the pressure recovery measured in the entrance of the other branch. Both of these phenomena are explained by the fact that the individual inlet-velocity ratios of the two branches of the duct were not necessarily the same as the system inlet-velocity ratio against which the pressure-recovery data are plotted because inlet A is subject to the type of twin-duct-flow instability discussed in reference 8. At inlet-velocity ratios less than 0.4 to 0.6, the inlet-velocity ratio of the branch of the duct with the high pressure recovery was substantially higher than the system inlet-velocity ratio; therefore the flow conditions of this branch of the duct were near those for maximum pressure recovery. The inlet velocity of the opposite branch of the duct was lower than the system inlet-velocity ratio and, as a result, the impact-pressure recovery was low.

The existence of flow instability is confirmed by measurements obtained by a surface-pressure orifice on the central body near the inlet of the duct containing the inlet rake (fig. 9). A discontinuity occurred in the variation with inlet-velocity ratio of the static pressure measured by this orifice when the system inlet-velocity ratio was reduced below that for maximum impact-pressure recovery as indicated by a survey of the pressure recovery in the venturi throat downstream of the junction of the two ducts (fig. 7). This discontinuity could be caused only by an abrupt change in the inlet-velocity ratio of the duct-branch entrance directly behind the orifice. At inlet-velocity ratios below 0.6 the duct branch

which contained the inlet rake was operating at a velocity ratio higher than the system inlet-velocity ratio and the other branch which contained the diffuser rake was operating at an inlet-velocity ratio lower than the system inlet-velocity ratio (fig. 9).

Since no static-pressure measurements were made inside the ducts, the individual inlet-velocity ratios of the two ducts of inlet A are not known. It was shown experimentally as well as analytically in reference 8, however, that, above the minimum inlet-velocity ratio for stable flow, the flow tends to divide evenly between the two ducts. The data presented herein therefore would be expected to be valid above this value of inlet-velocity ratio which, in the present case, is the value of the inlet-velocity ratio in figure 7 below which the impact-pressure recovery of either the inlet or diffuser first starts to decrease rapidly as the inlet-velocity ratio is reduced from the higher values. The value of minimum inlet-velocity ratio selected in this manner (see fig. 7) is approximately the same as the inlet-velocity ratio below which the average impact-pressure recovery measured in the venturi (downstream of the junction of the two branches of the ducts) also starts to decrease rapidly with decreases in the system inlet-velocity ratio.

Other tests (reference 7) have indicated that Mach number has no large effect on the minimum inlet-velocity ratio for high pressure recovery. The high Mach number data of figure 7 indicate high pressure recovery down to an inlet-velocity ratio of 0.5, and the low-speed tests of reference 1 at a comparable Reynolds number (short conical nose) indicated high recovery at the inlet above an inlet-velocity ratio somewhere between 0.4 and 0.6.

Substantial losses resulting from flow separation from the inner surface of the inlet lip were measured in the diffuser at the highest inlet-velocity ratios (fig. 5(b), $M_o = 0.40$). These losses become important for the take-off and climb conditions. Numerous experiments have shown, however, that such losses may be substantially reduced by the use of less curvature at the inlet lip.

At all Mach numbers except 0.40 the pressure recovery in the diffuser dropped precipitously at the maximum inlet-velocity ratio as a result of choking at the inlet. Impact-pressure measurements downstream of the inlet indicate substantial losses across the entire duct at this condition, (figs. 5(b) and 7). As the exit area was increased beyond that for choking at the inlet, the losses after diffusion progressively increased with the progression of the normal shock down the diffuser, while the inlet-velocity ratio remained constant. (See fig. 5(b), $M_o = 1.19$, $\frac{V_1}{V_o} = 0.76$.)

Inlets B and C.- Pressure-recovery curves are presented in figure 8 for the annular inlets B and C. Despite the scarcity of test points in

[redacted]

some cases, indicative curves can be drawn if it is admitted that the Mach number difference of the curves for each inlet has small effect on the minimum inlet-velocity ratio for high pressure recovery. Although the data do not permit a reliable conclusion to be drawn concerning the relative performance of inlets B (conical nose) and C (curved nose), the maximum pressure recovery shown by the highest test points for inlet B appears to be slightly higher than the maximum recovery shown for inlet C. The single test point at $\frac{V_1}{V_0} = 0.47$ for inlet B at the supersonic Mach number appears to indicate that high pressure recovery may be maintained to an inlet-velocity ratio slightly lower than that for inlet C. These fragmentary results seem to indicate that the central-body shape of inlet B is slightly better than for inlet C insofar as the pressure-recovery characteristics of the inlet are concerned.

The inlet-velocity-ratio range for near maximum pressure recovery is indicated in figure 8 to be appreciably less for inlet C than for inlet B. This difference is caused in part by the higher inlet-velocity ratio required in the case of inlet C to avoid boundary-layer separation from the central body ahead of the inlet and in part by the lower choking inlet-velocity ratios indicated for inlet C. It is pointed out that the differences in the indicated choking inlet-velocity ratios for inlets B and C probably are a result of the previously mentioned inaccuracy in measuring inlet-velocity ratio for choked inlet conditions rather than an actual difference in the choking inlet-velocity ratios of the two inlets. Reference to figure 4 shows that the corresponding differences in mass-flow coefficient A_0/A_1 are less than approximately 3 percent.

Effect of fixed transition on pressure recovery.- Inasmuch as boundary-layer transition may be expected to occur relatively farther forward on a full-scale aircraft than on the model tested, a transition strip was applied to the nose of inlet A in one test to insure transition well ahead of the inlet. Average-impact-pressure recoveries measured at two Mach numbers are presented in figure 10 and are compared with corresponding average-impact-pressure recoveries measured with natural transition. In each case the transition strip caused a slight reduction of the maximum-impact-pressure recovery coefficient. At the Mach number of 0.9 for the run with the transition strip, the flow distribution between the two branches of the duct happened to be reversed from that shown for the aerodynamically smooth configuration; these data, therefore, cannot be used for determining the effect of fixing transition on the minimum inlet-velocity ratio for high pressure recovery. Fortunately, however, the flow distribution between the two branches of the duct was the same with and without transition at the Mach number of 1.19. The curves of figure 10 for $M_0 = 1.19$ seem to indicate that the addition of the transition strip had only a small effect on the minimum inlet-velocity ratio for high pressure recovery. All the higher Mach number data presented, therefore, would be expected to be valid at full-scale Reynolds numbers.

[redacted]

External Pressure Distributions

Pressure distributions measured on the external cowling surface downstream of the inlet are presented in figure 11. As was mentioned in the discussion of the pressure-recovery measurements, the values of inlet-velocity ratio shown for inlet A (fig. 11(a)) are calculated from the total mass flow passing through both ducts, and the individual inlet-velocity ratio of either of the twin inlets is not known below system inlet-velocity ratios of about 0.5 or 0.6.

At a Mach number of 0.4, the flow phenomena are essentially the same as those discussed in reference 3. At the higher inlet-velocity ratios, the pressure distributions were nearly flat. As the inlet-velocity ratio was decreased, the pressure distributions changed, as would be expected from consideration of the relation between local angle of attack at the lip and inlet-velocity ratio. At the lowest inlet-velocity ratios, very high negative pressure peaks were measured near the inlet lip. In some cases, the manometer board height was insufficient to measure these pressures (fig. 11(a)), and these points are indicated by arrows on the pressure-distribution diagrams. Flow separation over the cowling is indicated by those curves for low inlet-velocity ratios which exhibit a relatively broad region of high negative pressure coefficient near the lip.

The critical Mach number, defined as the Mach number at which local sonic velocity is first attained in the flow over the cowling, could easily be exceeded at low Mach numbers by reducing the inlet-velocity ratio to those values for which large negative pressure peaks were induced at the inlet lip. However, because of the small extent into the stream of any shock present in this region (reference 9), appreciable shock losses and an associated drag increase are not necessarily expected when these pressure peaks at the inlet lip substantially exceed the critical pressure coefficient. A normal shock causing important drag increases is indicated in some cases where pressures substantially lower than the critical pressure increase to values corresponding to subsonic velocities near or downstream from the fuselage maximum diameter.

For Mach numbers of 0.90 and lower, the pressure distributions of inlet A (fig. 11(a)) show a compression to approximately free-stream pressures slightly downstream from the fuselage maximum diameter. At the Mach numbers of 0.94 and 1.19, this compression moved farther downstream beyond the last surface orifice on the model.

At those inlet-velocity ratios for which a nearly flat pressure distribution is shown, the induced velocities over the more gradually curved (and higher design critical Mach number) cowlings of inlets B and C (figs. 11(b) and 11(c)) were substantially lower than those of inlet A (fig. 11(a)). Consequently, for any specified supercritical Mach number, the critical pressure coefficient was not exceeded near the maximum diameter

[redacted]

station by inlets B and C to as great a degree as by inlet A. The shock losses and drag of inlets B and C would therefore be expected to be lower than those for inlet A.

A comparison of the external pressure distributions of inlets B and C at several inlet-velocity ratios is shown by cross plots in figure 12. Higher pressures are indicated over the external surface of the nose inlet with the curved central body (inlet C) as a result of the smaller effective lip angle of attack. The difference in the shape of the central bodies, however, had little influence on the pressures near the maximum diameter; hence, the external drag of the two arrangements would not be expected to differ importantly at the higher inlet-velocity ratios.

Wake-Survey Drag

Inlet-velocity-ratio effects.- Results of the drag measurements made with the external survey rake are presented in figure 13 as a function of inlet-velocity ratio. At any particular Mach number, the drag was smallest at the highest inlet-velocity ratios, where the drag also was relatively insensitive to inlet-velocity ratio. It will be remembered that below inlet-velocity ratios of approximately 0.6, the slopes of the curves for inlet A are doubtful since the data points are plotted as a function of the system inlet-velocity ratio.

The source of the enormous increases in drag which resulted when the inlet-velocity ratio was reduced from the higher values may be seen by examination of the external pressure distributions and wake profiles. The wake profiles are presented in figure 14 as the radial variation of point drag coefficient, which is the elemental drag coefficient calculated from the flow momentum defect at a point.

The boundary layer of the external surface was very thin at the low-drag high-inlet-velocity-ratio condition, but for those low-inlet-velocity ratios at which the large drag increases were measured, separation of the flow from the external surface at the inlet lip is evidenced by very large increases in the boundary-layer thickness shown by the wake profiles. A good example is provided by the data of inlet A for the Mach number of 0.4. As the inlet-velocity ratio was reduced from the maximum value to 0.57, the drag coefficient increased slightly (fig. 13(a)), and a sharp local pressure peak formed at the inlet lip (figure 11(a)). At lower inlet-velocity ratios, this sharp pressure peak dropped off and broadened, signifying separation, and the drag increased greatly. The wake profiles (figure 14(a)) show a corresponding large increase in the magnitude and extent of the boundary-layer losses.

Because of the smaller effective lip angle of attack induced by the curved central body, external-flow separation and the resulting large

[redacted]

drag increase were delayed to a lower inlet-velocity ratio for inlet C (figs. 13(b), 14(b), and 14(c)) than for inlet B. The central body of inlet C therefore appears to be preferable to the central body of inlet B with regard to the minimum inlet-velocity ratio that can be used without incurring large increases in external drag.

Shock losses.- A large increase in the wake-survey drag coefficient at the higher inlet-velocity ratios was measured for inlet A (fig. 13(a)) as the Mach number was increased from subcritical speeds to 0.94. The compression shock causing this drag increase is evidenced by the small but extensive loss shown in the wake profiles at the higher Mach numbers (fig. 14(a)), and by the supercritical pressures which increase to values corresponding to subsonic flow in the region near or downstream from the maximum diameter station (fig. 11(a)). As was inferred from the pressure distributions, the shock losses of the higher critical-speed inlets B and C (figs. 14(b) and 14(c)) are smaller and less extensive than those of inlet A.

The variation of the wake-survey drag coefficient with Mach number for inlets A and B is presented in figure 15 for inlet-velocity ratios of 0.6, which is near the minimum for high pressure recovery, and 1.0. This figure was obtained by cross-plotting the curves of figure 13. The drag of inlet A for both inlet-velocity ratios rose sharply above a Mach number of about 0.8, beyond which there was little difference in the drags for these inlet-velocity ratios.

At the Mach number of 0.8 for both inlet-velocity ratios, the drag of inlet A was approximately equal to that of inlet B. Data are not available over a range of inlet-velocity ratios for inlets B and C at Mach numbers other than 0.8. However, inasmuch as the curves of figure 13 show that very little change in drag resulted when the inlet-velocity ratio was increased above 1.0, drag values measured only at the maximum test inlet-velocity ratios at higher Mach numbers are plotted for inlet B in figure 15 and may properly be used for defining the curve for the inlet-velocity ratio of 1.0. This curve then shows that the drag of inlet B has risen but slightly up to a Mach number of 0.94, and is there much smaller than the drag of inlet A. It seems likely that the relationship between the drags of inlets A and B at the inlet-velocity ratio of 1.0 would be unaltered at the inlet-velocity ratio of 0.6. These results emphasize the importance of using a high-critical-speed cowling shape.

The flagged symbols in figure 15 for inlet A at the Mach number of 0.9 are for the case where transition was fixed on the central body and inlet lip. The differences in the locations of these symbols indicate the drag increase which resulted from the transition strip. This drag increase is of the magnitude that would be expected due to the elimination of laminar flow on the cowling surface.

[redacted]

For the three nose inlets of references 7 and 9 it was found that sharp pressure peaks induced at the inlet lip at low-inlet-velocity ratios resulted in no appreciable effect on the drag at subsonic Mach numbers above the critical Mach number. Wake-survey measurements indicated that the shock losses were essentially unaffected by the pressure peak in spite of the local supersonic Mach numbers indicated by the peak. This same phenomenon is shown by the data of inlet A for the Mach number of 0.79 and by the data of inlets B and C for the Mach number of 0.80 (figs. 11 and 14).

Consider the case of inlet A. A sharp pressure peak was measured at the inlet lip at a system inlet-velocity ratio of zero (fig. 11(a)). This pressure peak corresponds to a relatively high local supersonic Mach number from which the flow was gradually compressed to subsonic velocities. An inspection of the wake profiles for this Mach number (0.79) shows no evidence of shock losses (fig. 14(a)) with the high negative peak pressure coefficient present $\left(\frac{V_1}{V_o} = 0\right)$ but indicates that the drag increase shown in figure 13(a) results from external separation of the flow at the inlet lip. A different behavior is indicated by the data for Mach numbers of 0.85 and 0.90, however. It is shown in figure 11(a) that the Mach number ahead of the normal shock, and consequently the losses through this shock, were increased as the inlet-velocity ratio was reduced to very low values. This phenomenon is illustrated by the wake profile for the Mach number of 0.90 (fig. 14(a)) where it is seen that the large drag increase measured at zero inlet-velocity ratio is due in large part to the increased shock losses.

The magnitude of the drag increase caused by reducing the inlet-velocity ratio will be appreciated when compared with the drag of a complete airplane. The drag coefficient of the D-558-II airplane, for example (reference 10), varies from values of approximately 0.02 to 0.08 through the transonic speed range (based on wing area). The maximum increase in the wake-survey drag coefficient for inlet A, M = 0.9 (fig. 13(a)) which resulted from reducing the inlet-velocity ratio to approximately 0.1 from the higher values was 0.024 (based on wing area).

Supersonic External Pressure Drag

The relative external pressure drags of inlets A and B at the supersonic test Mach number have been estimated from the external pressure distributions with the assumption that the presence of the pilot's canopy and nose-wheel fairing of inlet A had no large effect on the pressures at the row of pressure orifices. The method of calculating the external pressure-drag coefficient is discussed in the section entitled "Methods and Precision," where it was shown that the calculation required

knowledge of the force on the central body. Inasmuch as no surface pressures were measured on the central bodies with the exception of that measured by the single pressure orifice previously mentioned, the comparison of the external pressure drags of inlets A and B is made by comparing for each inlet the value of the external pressure-drag coefficient less the central-body force coefficient. Inlets A and B had the same central body, so that the force on the central body at any given inlet-velocity ratio should be the same for each inlet, and the difference in the quantity $\left(C_{D_p} - C_{F_c}\right)$ for each inlet at a given inlet-velocity ratio would therefore be the difference in the external pressure-drag coefficients. The quantity $\left(C_{D_p} - C_{F_c}\right)$ is presented as a function of inlet-velocity ratio in figure 16, where it is indicated that the external pressure drag of inlet B is substantially lower than that of inlet A.

In order to estimate roughly the magnitude of the pressure-drag coefficients of inlets A and B and compare these magnitudes with those of other bodies, the force on the conical central body of inlets A and B was estimated at an inlet-velocity ratio of 0.6. The pressure acting on the conical central body from the apex to the normal shock ahead of the inlet was calculated from knowledge of the cone angle and free-stream Mach number. The pressure was assumed to jump suddenly at the shock position to the value given for a normal shock from the supersonic Mach number on the cone. The pressure on the central body at the inlet was assumed equal to the value calculated from the one-dimensional value of inlet-velocity ratio. Between the shock position and the inlet, the pressure was simply assumed to vary linearly when plotted as a function of the square of the central-body radius. (The pressure measured by the only available nose-pressure orifice agreed well with this assumed distribution.)

The external pressure-drag coefficients obtained by adding the estimated central-body force coefficient to the values of $C_{D_p} - C_{F_c}$ for inlets A and B at an inlet-velocity ratio of 0.6 are shown in figure 16. The two points shown for each inlet correspond to two different assumptions of the shock position as indicated by the shadowgraph observation. The higher points were calculated with the normal shock assumed $1\frac{1}{2}$ inches ahead of the inlet, and the lower points were calculated with the shock assumed 1 inch ahead of the inlet. The pressure drags of the NACA 1-40-200 nose inlet and a solid elliptical nose of ellipsoid fineness ratio 6 (major-to-minor axis ratio) are presented for comparison in figure 16. These data were obtained from reference 7. Inlet A is indicated to have the highest drag of all configurations, and the drag of inlet B is approximately equal to that of the NACA 1-40-200 nose inlet, which is about 30 percent higher than that of the closed-nose body.

[redacted]

Design Considerations

The results of the investigation indicate that the inlet arrangements investigated achieve the objective of avoiding important adverse boundary-layer interaction effects on the internal flow in the transonic range, at least up to a Mach number of 1.19. The configurations investigated obviously are not optimum, however.

The reduction in the external drag at transonic speeds which resulted from replacing the low critical Mach number nose inlet of inlet A with the more gradually curved, higher critical Mach number nose inlet of inlet B as well as the tests of references 7 and 9 suggest that further improvement in the transonic drag of the inlet may be effected by utilizing an external shape of still higher critical speed. As the curvature of the external surface is decreased to obtain lower induced velocities and higher critical speeds, other things remaining constant, the minimum inlet-velocity ratio needed to prevent a pressure peak at the inlet lip is expected to increase.

Since increasing the inlet-velocity ratio to the higher values needed to remove the pressure peaks on the inlet lip may reduce the ultimate pressure recovery, the improvement in the external characteristics must be compromised with the impairment of the internal characteristics. The gains to be realized in removing the pressure peak at the lip may be either very large or quite small. If the peak is quite localized at the lip with a rapid compression rearward, the only appreciably detrimental result may consist of a forward movement of the boundary-layer transition point, which for full-scale aircraft may involve a very small increase in drag. If the peak is broad, the flow may separate from the lip, or the strength of the normal shock on the external surface may increase with very large drag increases possible.

The present data also indicate that a small amount of curvature may be incorporated in the nose profile without affecting the internal pressure-recovery characteristics of the inlet appreciably. This curvature would provide increased volume in the nose and, at the same time, by reducing the effective flow angle at the lip, would reduce the value of inlet-velocity ratio required to avoid the formation of a pressure peak on the lip.

Further research is required to establish the optimum configuration of this type of inlet from the viewpoint of further increasing the pressure recovery and reducing the drag.

[redacted]

CONCLUSIONS

The following major conclusions were drawn from an investigation of three fuselage air inlets designed specifically to avoid important adverse boundary-layer shock-interaction effects on the internal-flow pressure recovery up to a small supersonic Mach number:

1. The maximum values of impact-pressure recovery coefficient were high (approximately 0.96 at the inlet of configuration A) and were little affected by Mach number over the range investigated, even for the supersonic Mach number 1.19.

2. A reduction of inlet-velocity ratio below the value for an approximately flat external pressure distribution led to reduced pressures over the external surface near the inlet lip. At the subsonic Mach numbers, these reduced pressures took either the form of a sharp peak in the distribution, with a rapid compression rearward and only a small increase in external drag, or a broader peak which was associated with very large drag increases. Wake surveys showed that these large drag increases resulted from separation of the external flow at the inlet lip and, in some cases, from increased shock losses.

3. External-flow separation at the inlet lip was delayed to a lower inlet-velocity ratio by substituting a curved nose for the conical nose of one configuration. This change led, however, to a small reduction in the maximum impact-pressure recovery.

4. At inlet-velocity ratios in the range of those suitable for high-speed operating conditions, the wake-survey drag coefficient of one configuration rose sharply above a Mach number of 0.8. The drag of another configuration which had an external shape of higher critical speed, increased very little up to a Mach number of 0.94.

5. The use of the external shape of higher critical speed resulted also in a substantial reduction in the external pressure-drag coefficient at the supersonic Mach number. The pressure drag of this configuration was estimated to be approximately equal to that of the NACA 1-40-200 nose inlet and 30 percent greater than that of a closed nose of fineness ratio 6.0.

Langley Aeronautical Laboratory
National Advisory Committee for Aeronautics
Langley Air Force Base, Va.

[redacted]

REFERENCES

1. Nichols, Mark R., and Rinkoski, Donald W.: A Low-Speed Investigation of an Annular Transonic Air Inlet. NACA RM L6J04, 1947.

2. Nichols, Mark R., and Gorla, Edwin B.: A Low-Speed Investigation of a Fuselage-Side Air Inlet for Use at Transonic Flight Speeds. NACA RM L7A06, 1947.

3. Baals, Donald D., Smith, Norman F., and Wright, John B.: The Development and Application of High-Critical-Speed Nose Inlets. NACA Rep. 920, 1948.

4. Ritchie, Virgil S., Wright, Ray H., and Tulin, Marshall P.: An 8-Foot Axisymmetrical Fixed Nozzle for Subsonic Mach Numbers up to 0.99 and for a Supersonic Mach Number of 1.2. NACA RM L50A03a, 1950.

5. Smith, Norman F.: Numerical Evaluation of Mass-Flow Coefficient and Associated Parameters from Wake-Survey Equations. NACA TN 1381, 1947.

6. Baals, Donald D., and Mourhess, Mary J.: Numerical Evaluation of the Wake-Survey Equations for Subsonic Flow Including the Effect of Energy Addition. NACA ARR L5H27, 1945.

7. Pendley, Robert E., and Robinson, Harold L.: An Investigation of Several NACA 1-Series Nose Inlets with and without Protruding Central Bodies at High-Subsonic Mach Numbers and at a Mach Number of 1.2. NACA RM L9L23a, 1950.

8. Martin, Norman J., and Holzhauser, Curt A.: Analysis of Factors Influencing the Stability Characteristics of Symmetrical Twin-Intake Air-Induction Systems. NACA TN 2049, 1950.

9. Pendley, Robert E., and Smith, Norman F.: An Investigation of the Characteristics of Three NACA 1-Series Nose Inlets at Subcritical and Supercritical Mach Numbers. NACA RM L8L06, 1949.

10. Osborne, Robert S.: High-Speed Wind-Tunnel Investigation of the Longitudinal Stability and Control Characteristics of a $\frac{1}{16}$-Scale Model of the D-558-2 Research Airplane at High Subsonic Mach Numbers and at a Mach Number of 1.2. NACA RM L9C04, 1949.

[redacted]

TABLE I.- CANOPY COORDINATES

(a) Water Lines

[All dimensions are in inches]

X	Z_p														
	WL 0.110	WL 0.220	WL 0.330	WL 0.440	WL 0.550	WL 0.660	WL 0.770	WL 0.880	WL 0.990	WL 1.100	WL 1.210	WL 1.320	WL 1.430	WL 1.540	WL 1.650
-1.628 -1.469 -1.280								0	0	0					
-1.100 -1.042 -.781								.195	.175	.119	0	0			
-.550 -.477 -.111								.346 .434	.301	.391	.358	.233	0		
-.103 0 .220									.517 .548	.556	.548	.484	.383 .483	0 .173 .301	
.330 .392 .440										.612					0
.550 .770 1.100								.515 .547	.580 .611			.615 .644	.537 .605	.418 .605	.190 .339
1.320 1.430 1.650							0.486 .486 .474	.550 .540	.615 .616 .606				.616 .614	.517 .517 .513	.359 .353
2.200 2.310 2.420						0.332	.410	.464	.584	.584			.572	.462	.274
2.730 2.816 3.080						.282	.308	.350	.394	.440			.508 .469	.378	.082 0
3.190 3.330 3.630				0.082	0.162 .146	.174	.204	.234	.264	.292				.283	
3.850 3.960 3.971			0.036	.060	.074	.086	.102	.116	.132	.147				.130 0	
4.180 4.290 4.400	0.004 0	0.012 0	0	0	0	0	0	0	0	0					

TABLE I.- CANOPY COORDINATES - Concluded

(b) Top of Canopy

$Z_p = 0$

X	WL
-1.650	0.803
-1.100	1.186
-.550	1.407
0	1.565
.220	1.615
.550	1.676
1.100	1.729
1.320	1.738
1.540	1.738
1.650	1.736
2.20	1.704
2.750	1.654
3.330	1.606
3.850	1.553
4.400	1.498

TABLE II.- NOSE-WHEEL-FAIRING COORDINATES

(a) Water Lines

[All dimensions are in inches]

X	Z_w															
	WL -0.095	WL -0.190	WL -0.285	WL -0.379	WL -0.474	WL -0.569	WL -0.664	WL -0.759	WL -0.854	WL -0.949	WL -1.043	WL -1.138	WL -1.233	WL -1.328	WL -1.423	WL -1.518
-1.124 -1.100 -.990									0 .016 .068							
-.982 -.824 -.692										0	0	0				
-.550 -.452 -.330										.226 .270	.186 .262	.098 .222	0 .130			
-.220 -.214 -.110													.220 .248	0		
0 .090 .110										.316	.320	.310	.284	.220 .248	0	
.220 .550 .770										.346 .348	.340 .356	.334 .350			.194 .220	0 .106
1.100 1.210 1.430									.322 .320	.348 .342	.362	.362				.132 .094
1.572 1.650 1.670								0.262	.312	.358	.354	.352				0
2.200 2.640 2.750							0.172 .154	.242 .184	.274 .212	.296 .222	.304 .227	.227				
3.190 3.330 3.520					0.060	0.102 .094	.110	.123	.140	.148	.151	.151				
3.850 4.070 4.180		0.006	0.014	0.030	.037	.046	.054	.062	.070	.072	.076	.076				
4.314 4.400	0.001 0	0	0	0	0	0	0	0	0	0	0	0				

NACA

TABLE II.- NOSE-WHEEL-FAIRING COORDINATES - Concluded

(b) Bottom of Wheel Well

$Z_W = 0$

X	WL
-1.100	-0.872
-0.550	-1.190
0	-1.396
.220	-1.454
.550	-1.516
1.100	-1.552
1.320	-1.540
1.430	-1.538
1.650	-1.508

NACA

[redacted]

TABLE III

CENTRAL BODY COORDINATES

[All dimensions are in inches]

Inlet A		Inlet B		Inlet C	
X	r_c	X	r_c	X	r_c
-5.973	0	-5.973	0	-5.973	0
0	1.001	0	1.001	-5.650	0.090
0.220	1.024	0.050	1.008	-5.250	.188
.550	1.008	.150	1.017	-4.850	.282
1.100	0.924	.250	1.018	-4.450	.370
1.650	.840	.350	1.015	-4.050	.456
2.200	.754	.450	1.011	-3.650	.539
2.750	.656	.550	1.005	-3.250	.614
3.330	.530	.650	.998	-2.850	.683
3.850	.348	.750	.992	-2.450	.744
4.400	0	1.110	.968	-2.050	.800
		1.650	.926	-1.650	.849
		2.200	.878	-1.250	.890
		2.750	.822	-0.850	.930
		3.333	.760	-.450	.965
		3.850	.572	-.250	.980
		4.400	0	0	1.001
				.050	1.005
				.150	1.010
				.250	1.012
				.350	1.010
				.450	1.008
				.550	1.003
				.650	.998
				.750	.992
				1.110	.968
				1.650	.926
				2.200	.878
				2.750	.822
				3.333	.760
				3.850	.572
				4.400	0

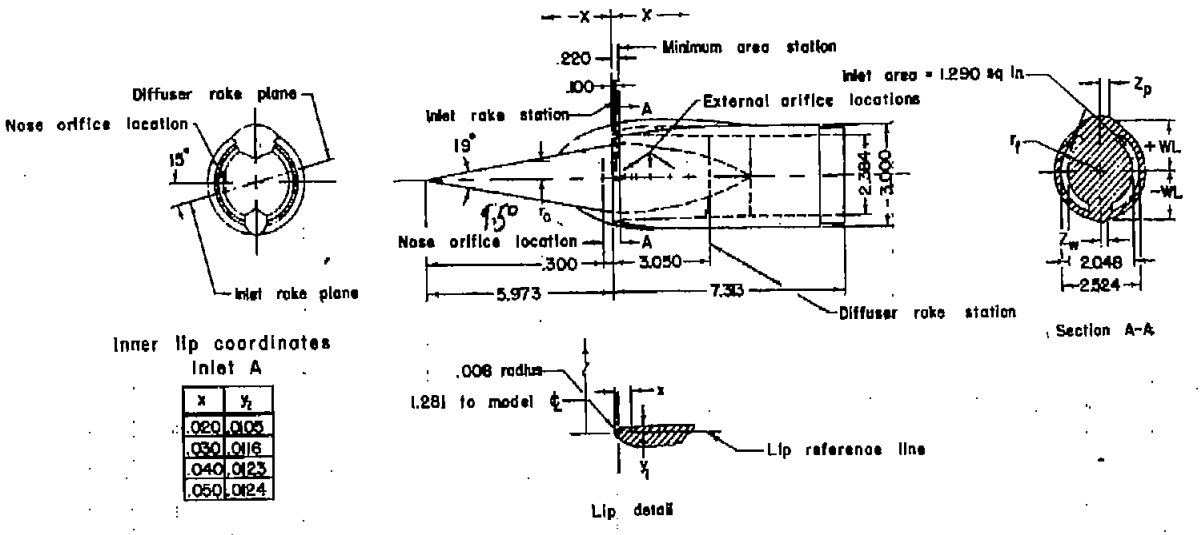

x	y_i
.020	.0105
.030	.0116
.040	.0123
.050	.0124

(a) Inlet A.

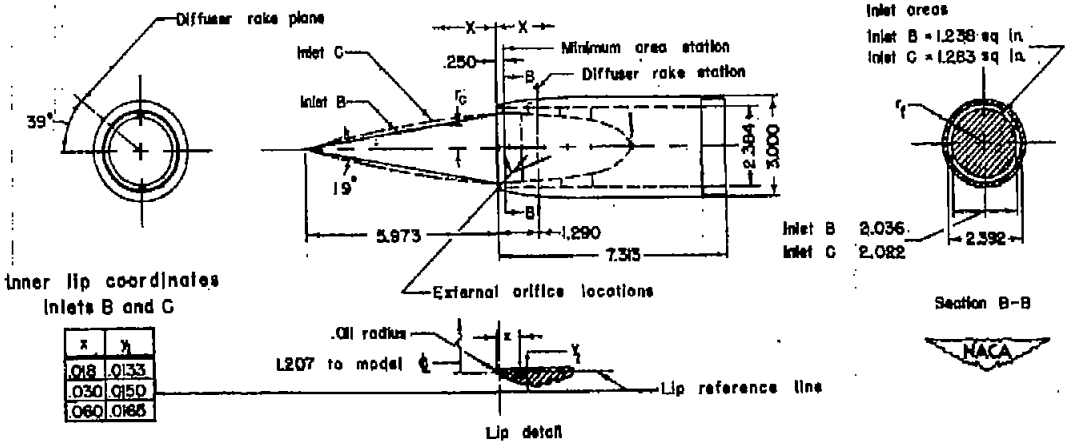

x	y_i
.018	.0133
.030	.0150
.060	.0165

(b) Inlets B and C.

Figure 1.- Model configurations investigated. (All dimensions are in inches.)

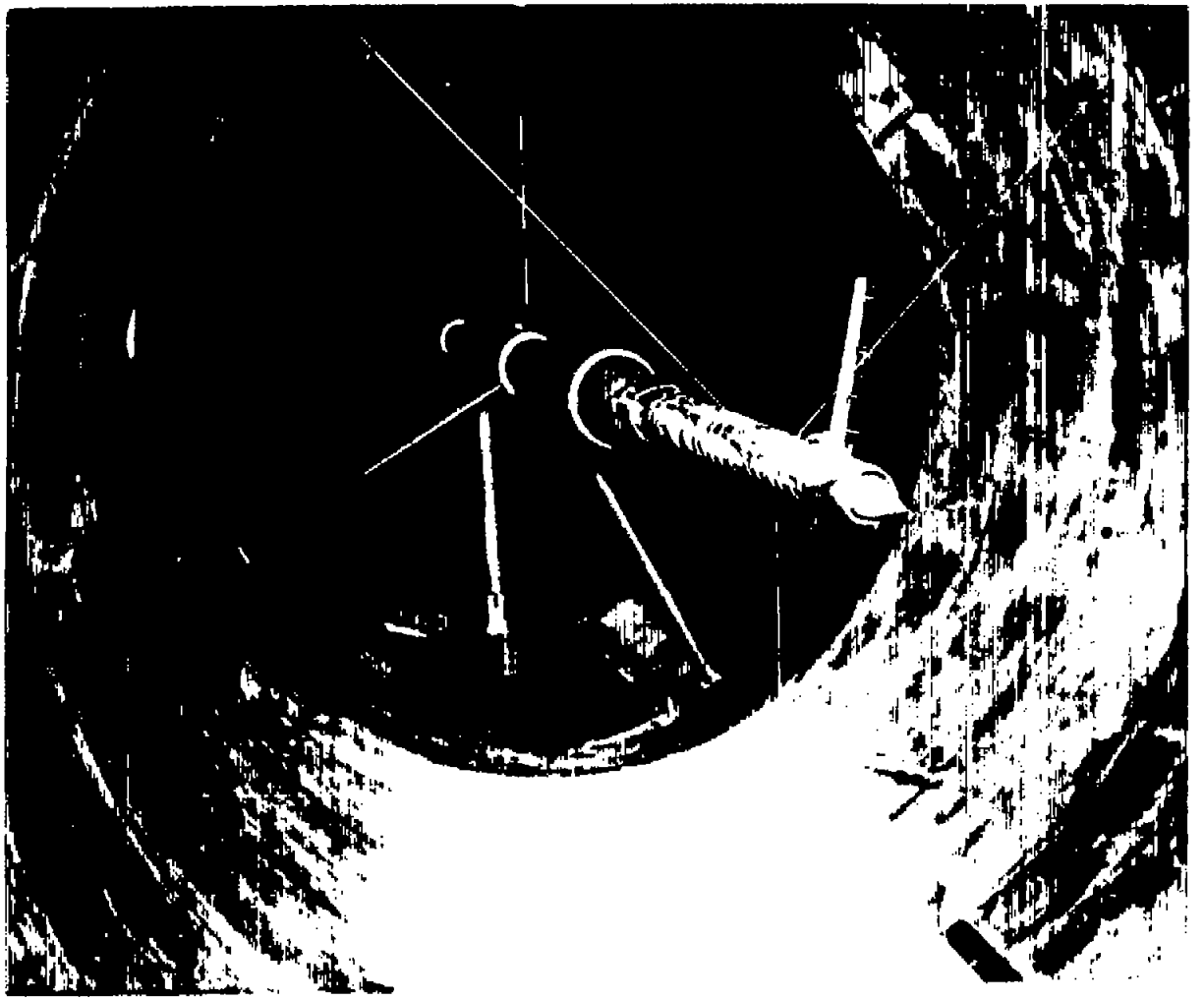

Figure 2.- Model installation in tunnel.

NACA
L-64026

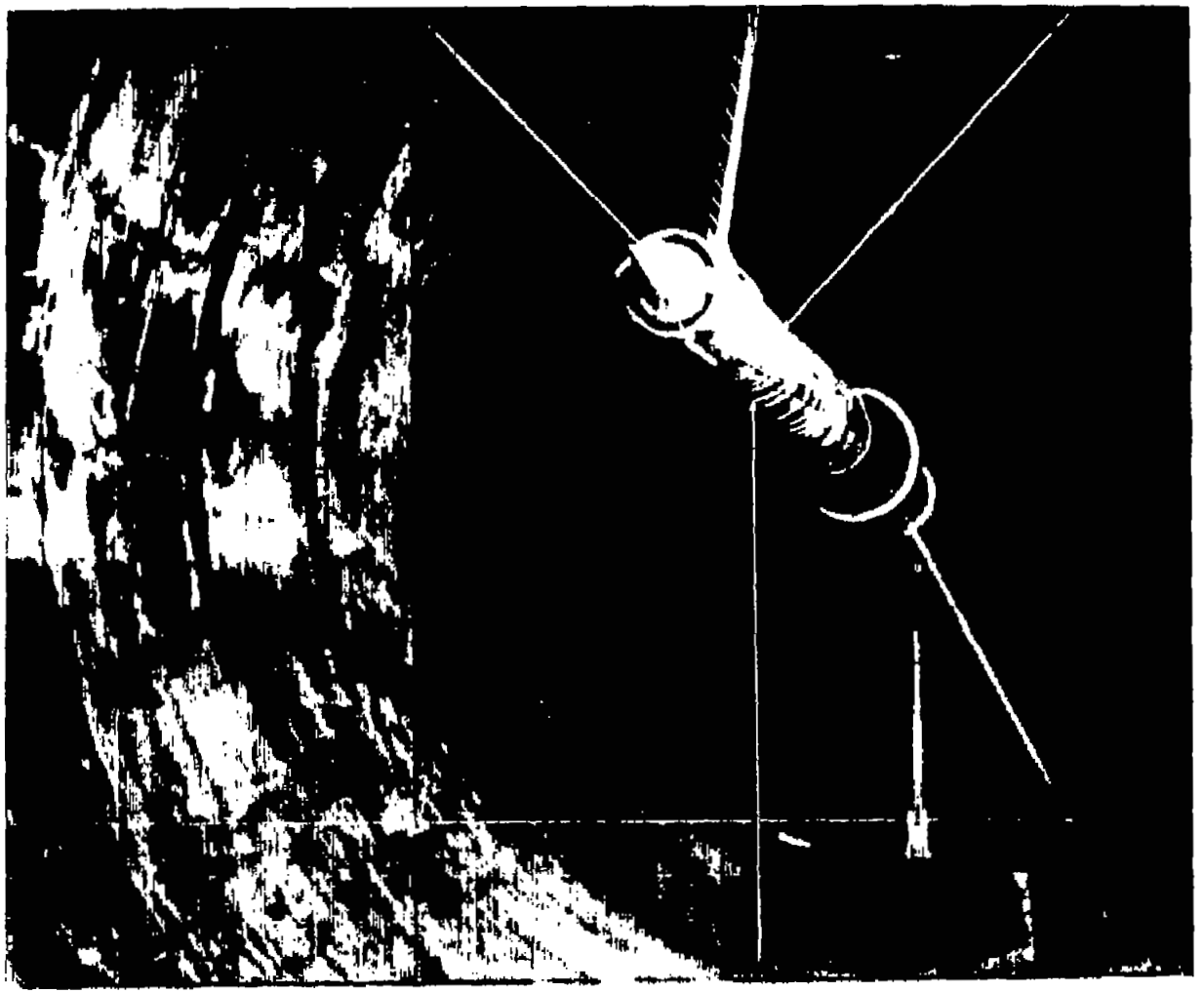

Figure 2.- Concluded.

NACA
L-64027

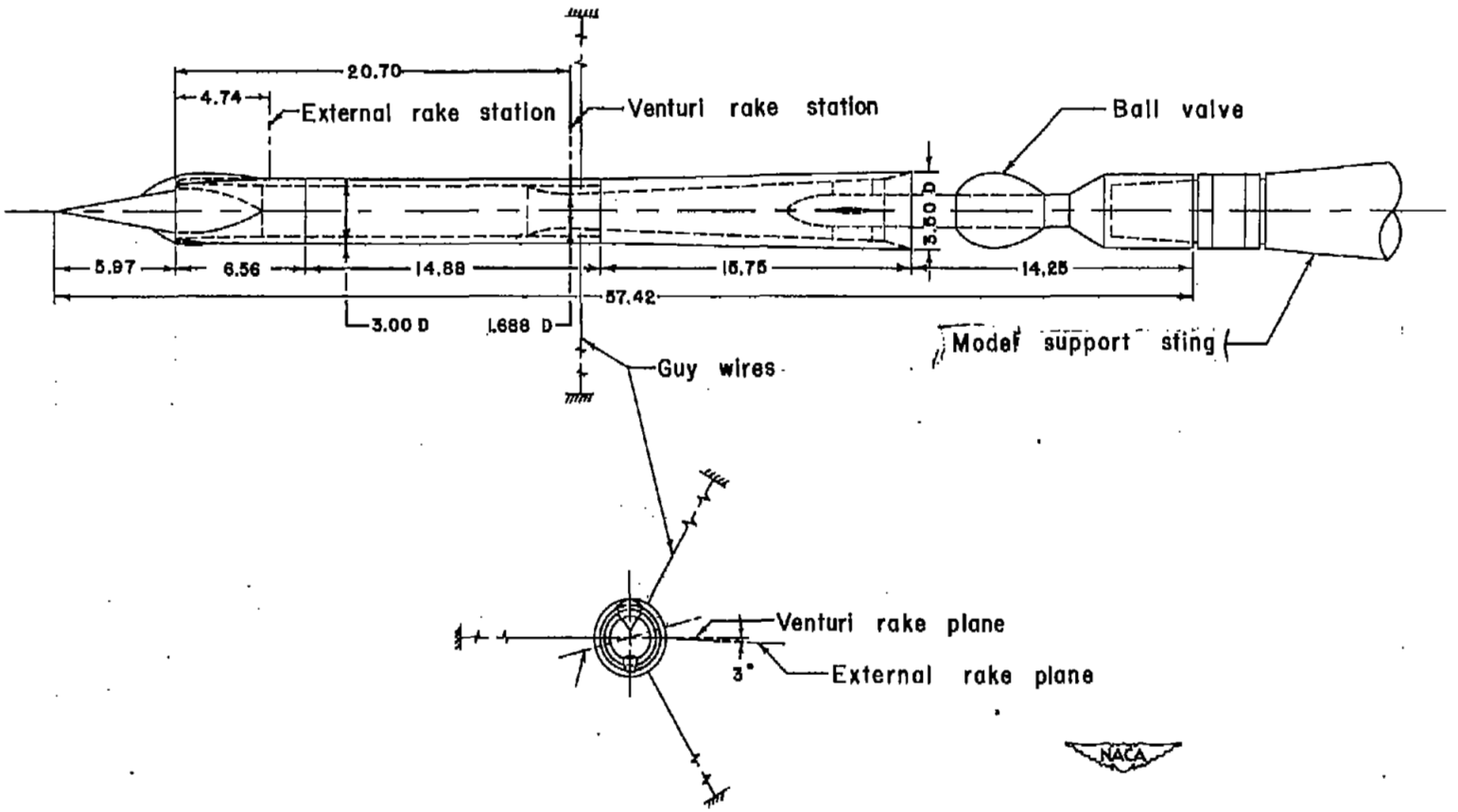

Figure 3.- Details of model installations. (All dimensions are in inches.)

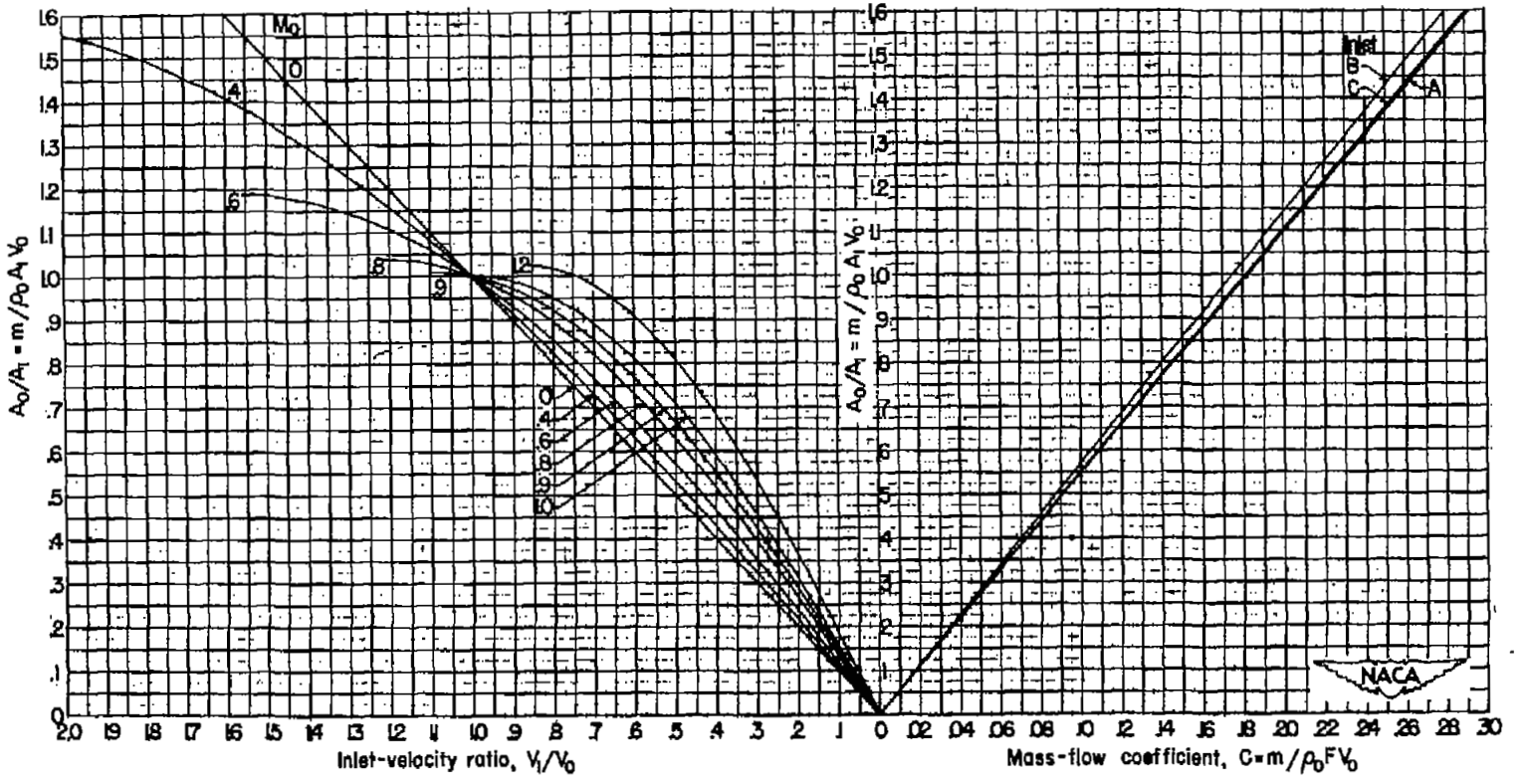

Figure 4.- Mass-flow coefficient - inlet-velocity ratio conversion chart.

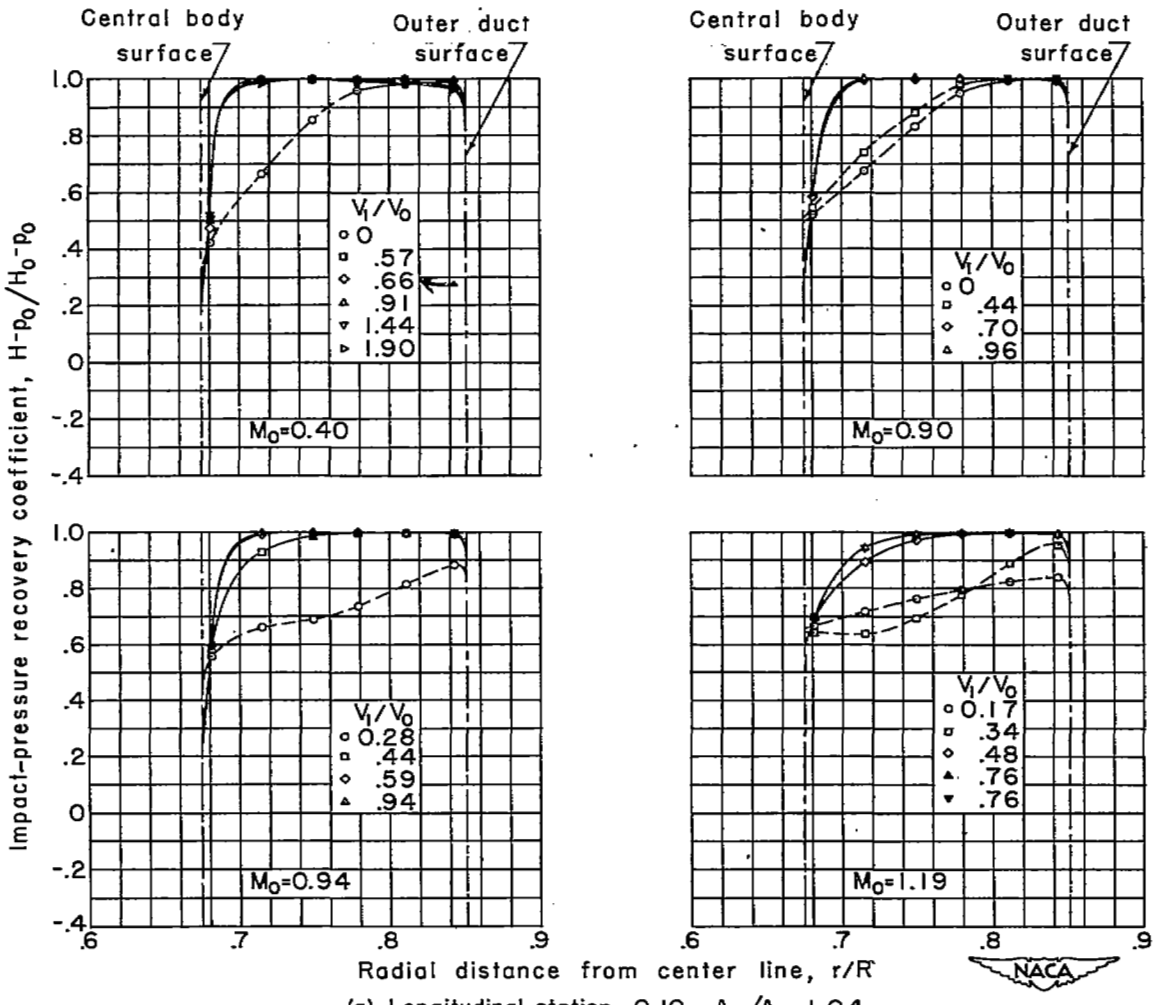

(a) Longitudinal station, 0.10; A_e/A_l, 1.04.

Figure 5.- Impact-pressure recovery distributions. Inlet A.

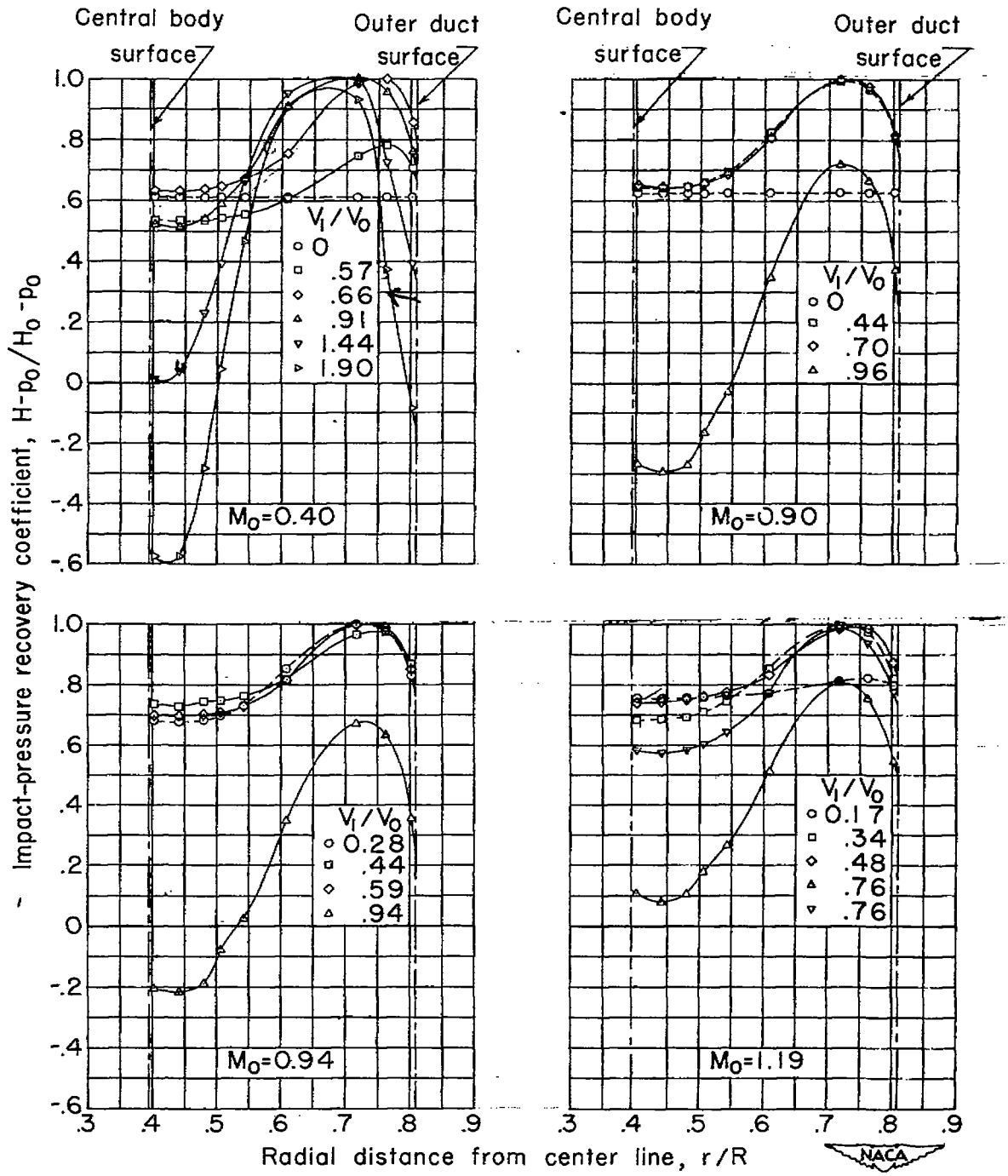

(b) Longitudinal station, 3.05; A_d/A_1, 2.31.

Figure 5.- Concluded.

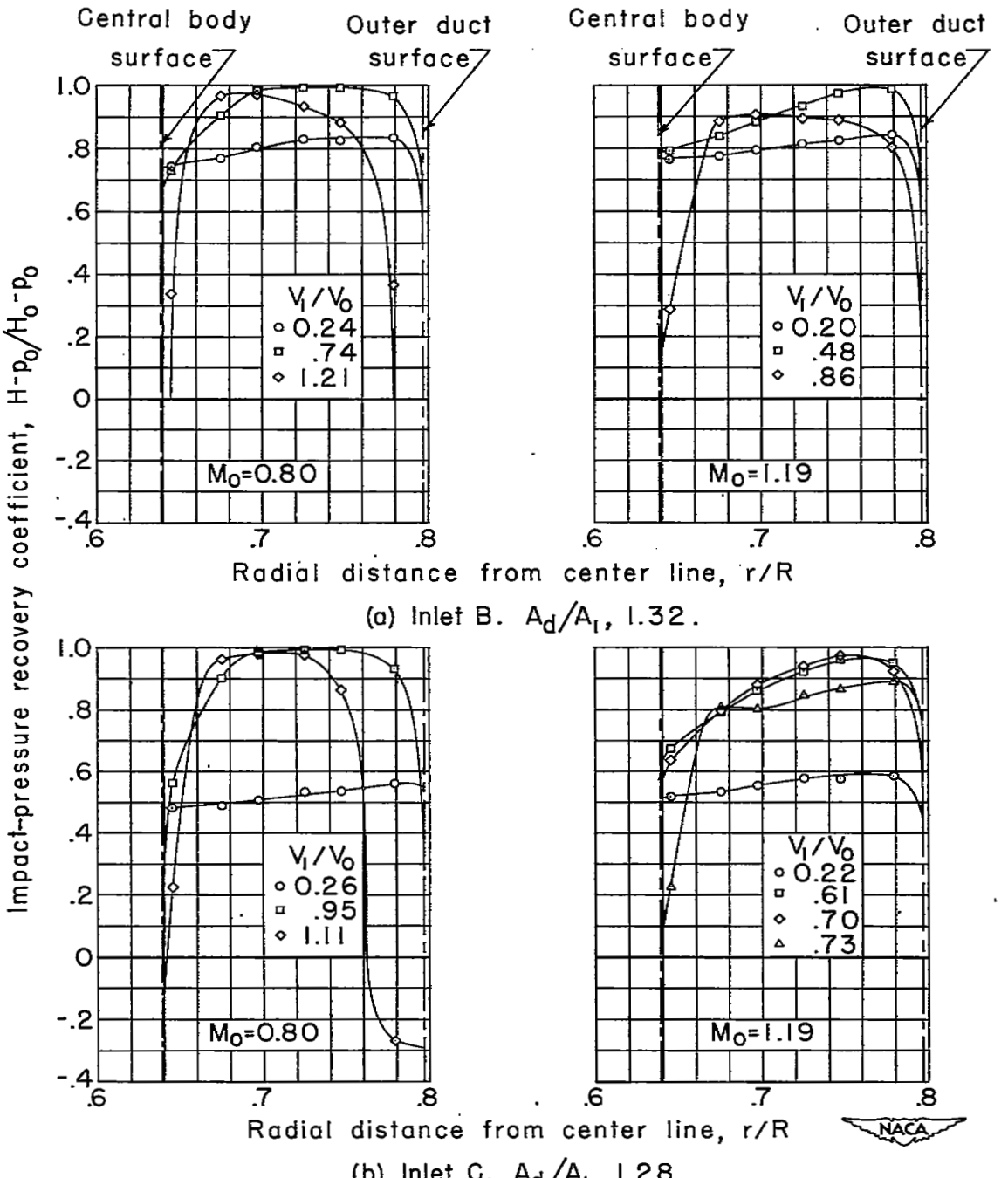

Figure 6.- Impact-pressure recovery distributions; longitudinal station, 1.29. Inlets B and C.

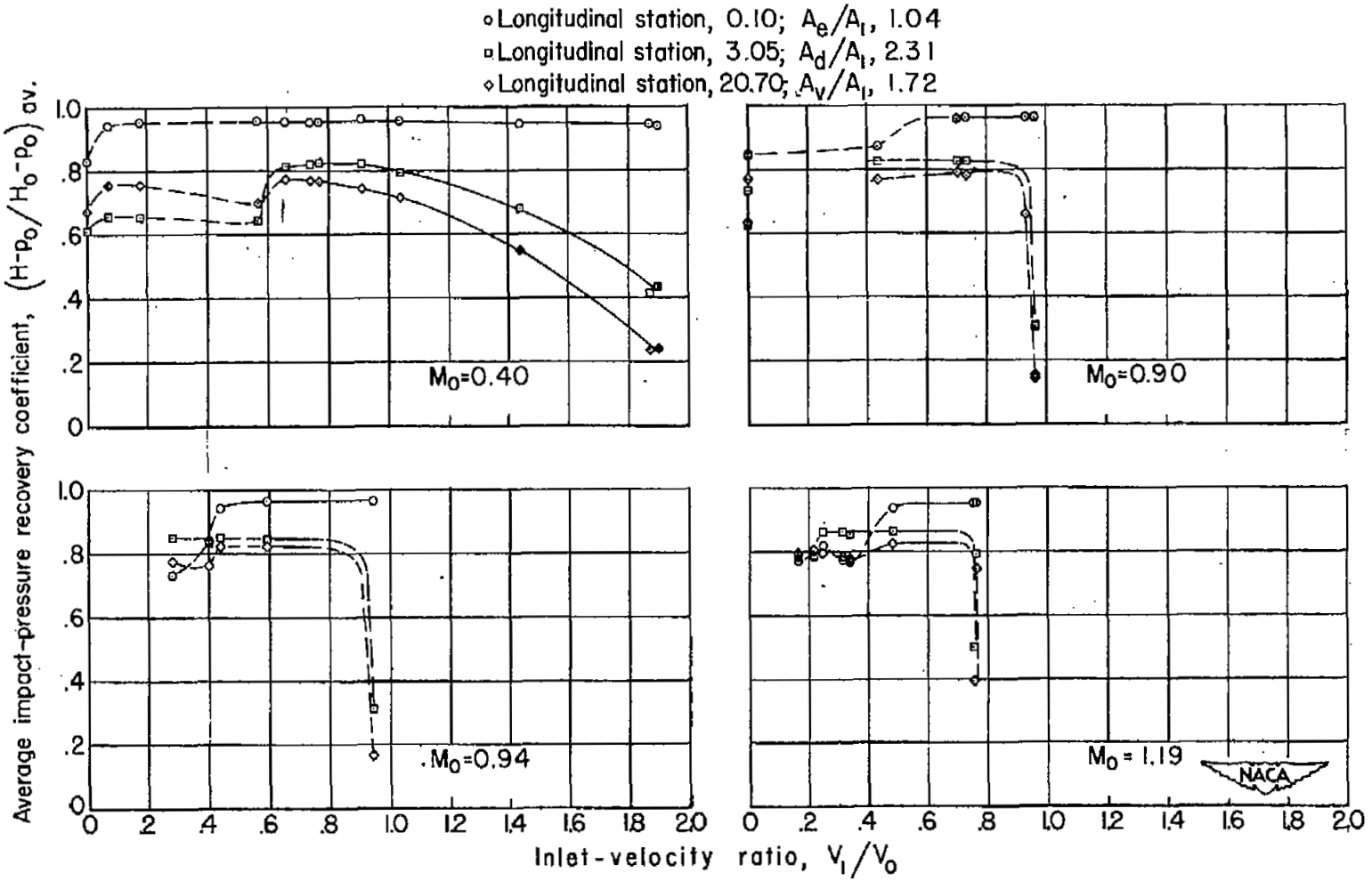

Figure 7.- Variation of average impact-pressure recovery with inlet-velocity ratio. Inlet A.

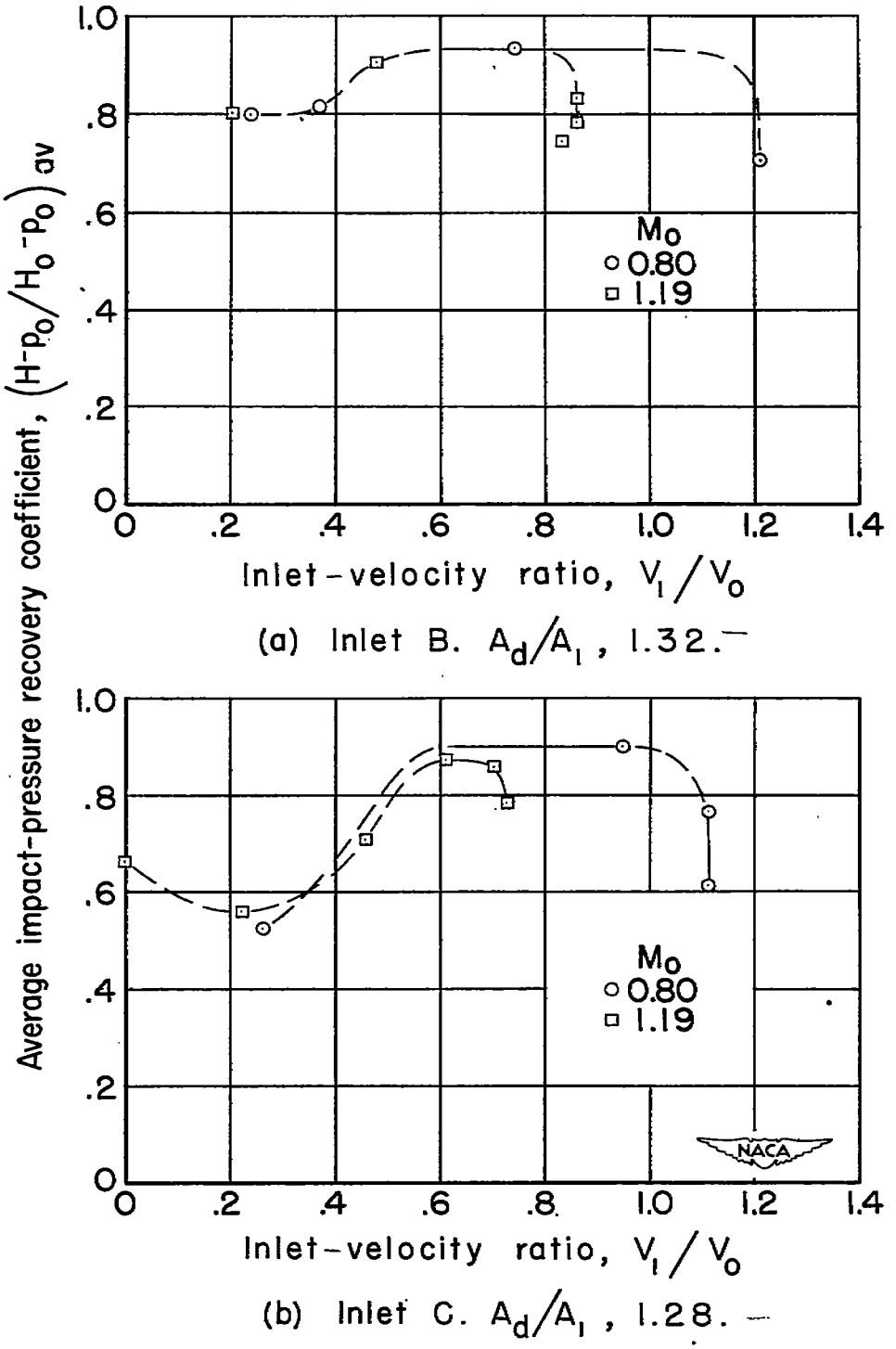

Figure 8.- Variation of average impact-pressure recovery with inlet-velocity ratio; longitudinal station, 1.29. Inlets B and C.

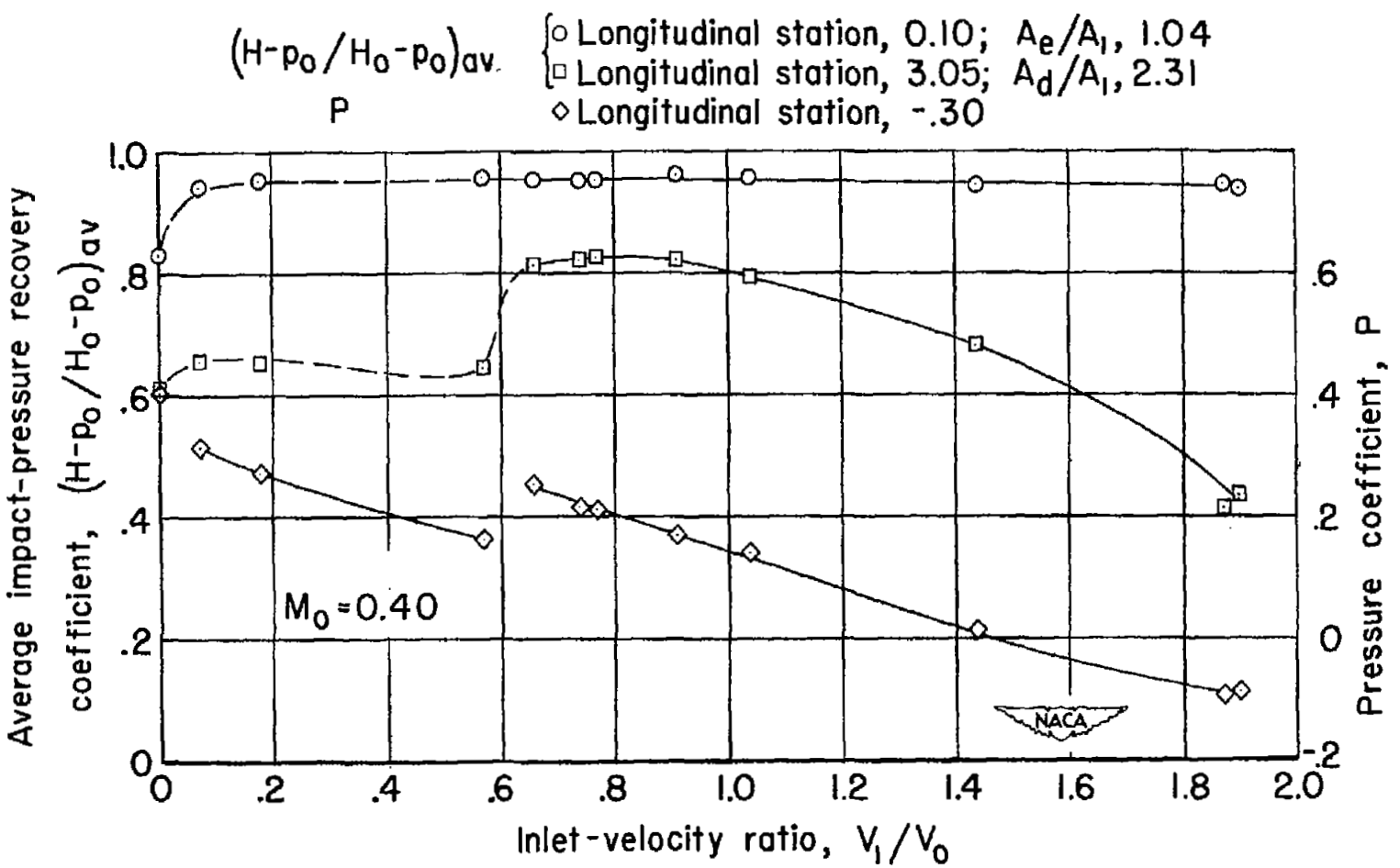

Figure 9.- Comparison of static-pressure variation near inlet with that of average impact-pressure recovery coefficient. Inlet A.

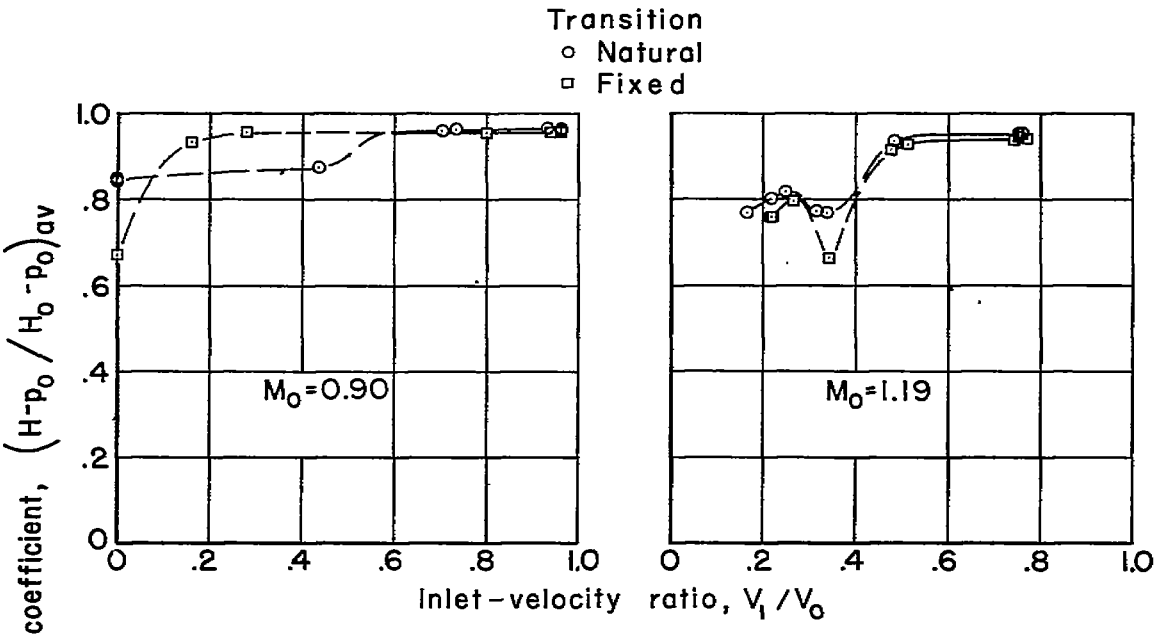

(a) Longitudinal station, 0.10; A_e/A_i, 1.04.

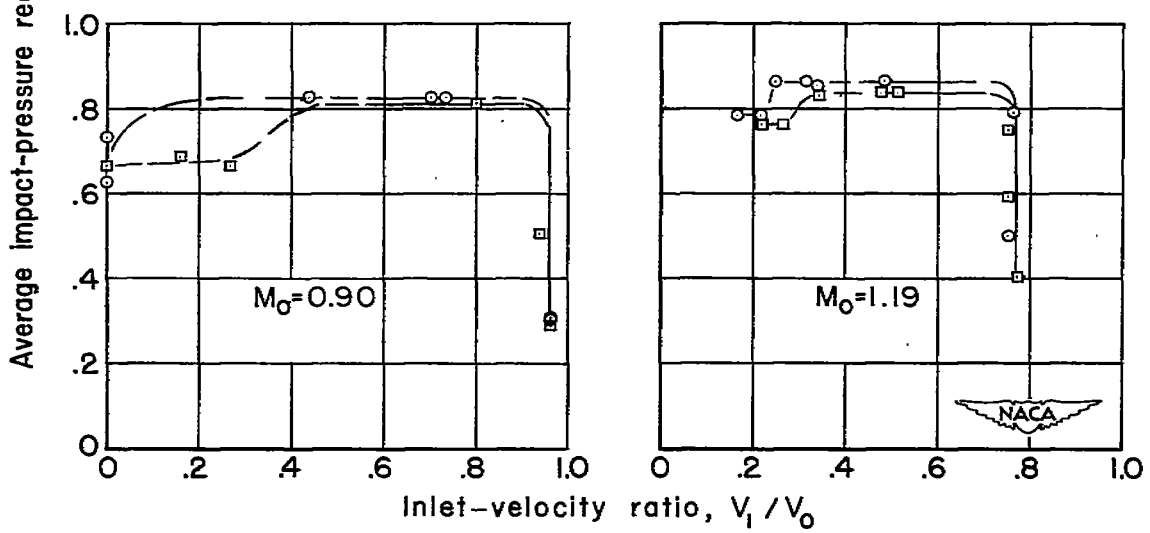

(b) Longitudinal station, 3.05; A_d/A_i, 2.31.

Figure 10.- Effect of fixed transition on average impact-pressure recovery. Inlet A.

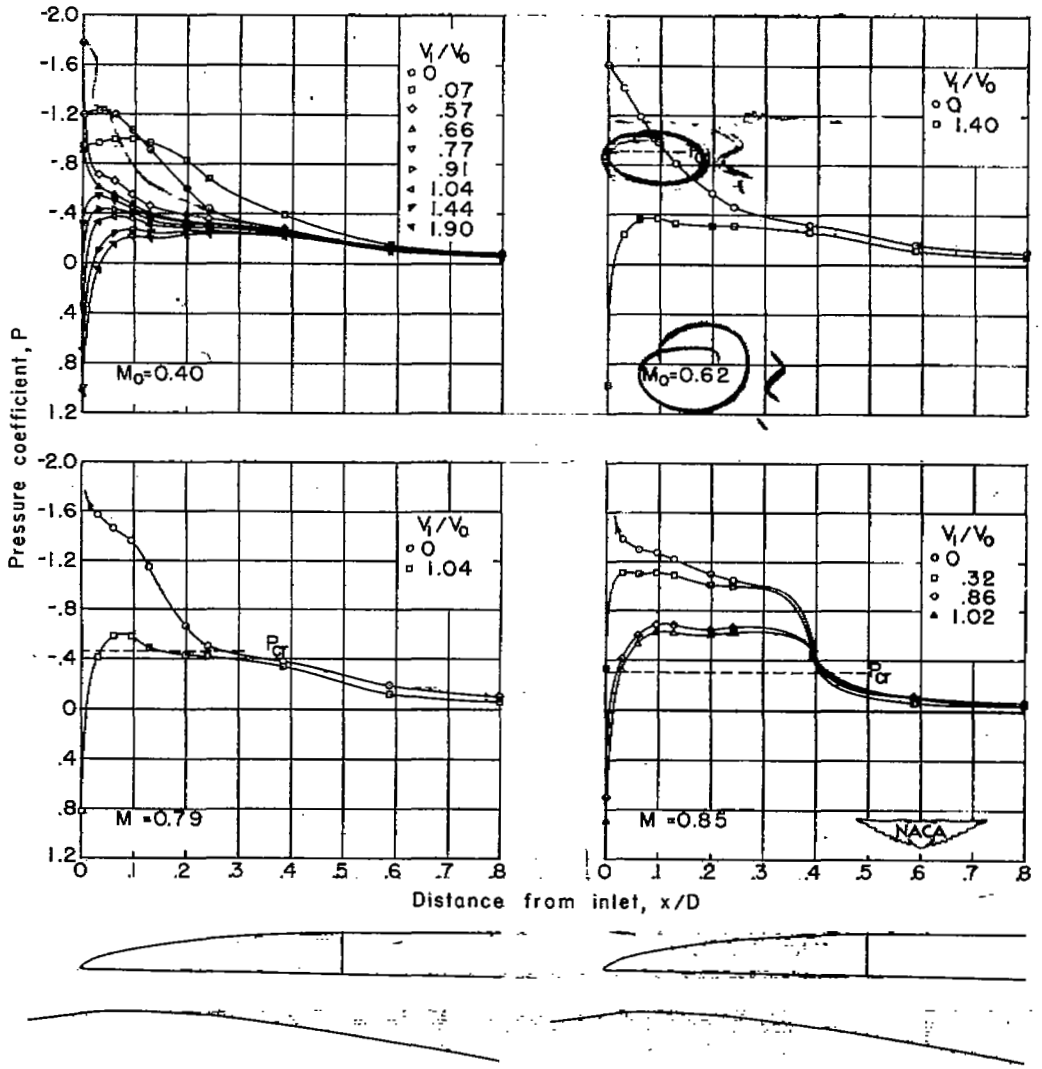

(a) Inlet A.

Figure 11.- External-surface pressure distributions.

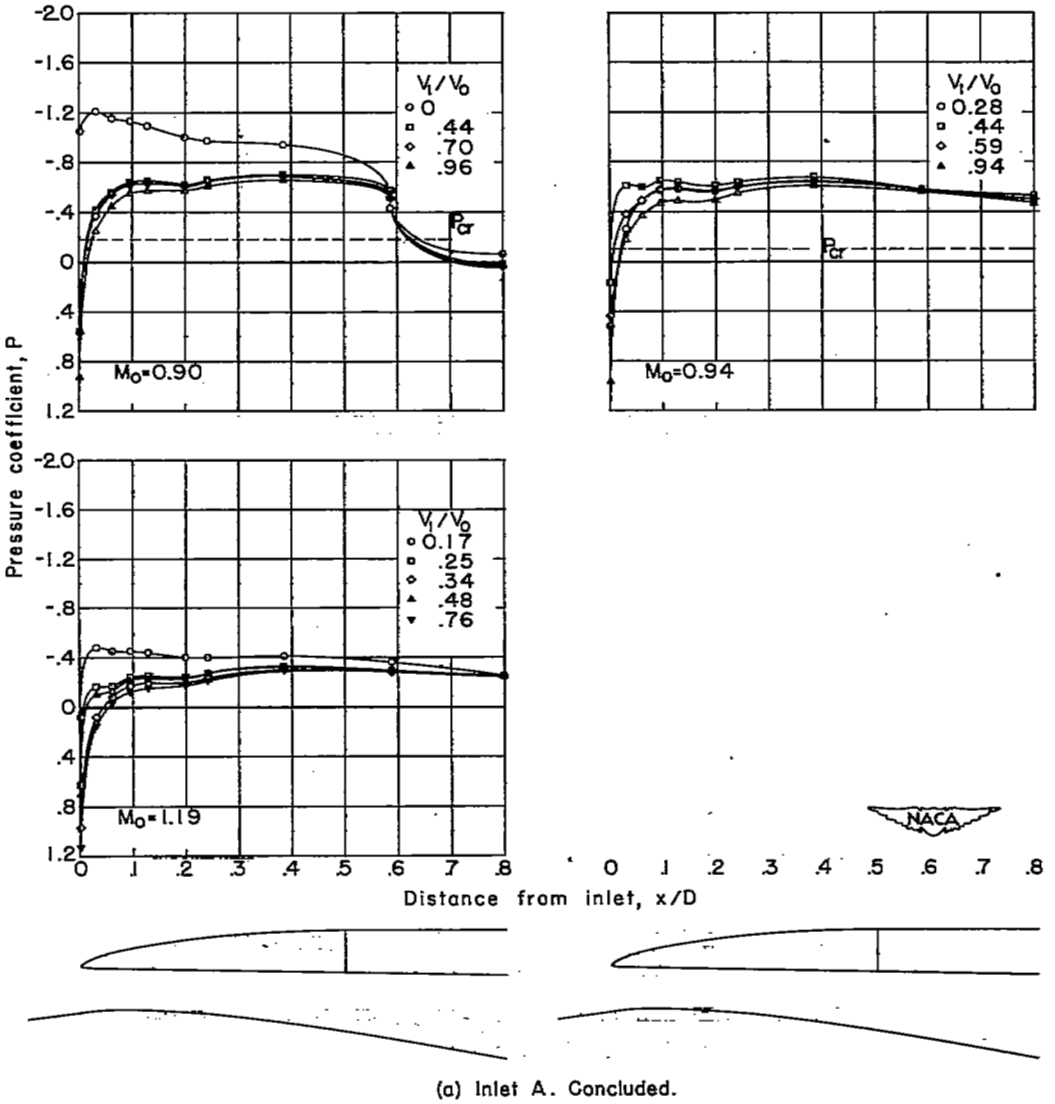

(a) Inlet A. Concluded.

Figure 11.- Continued.

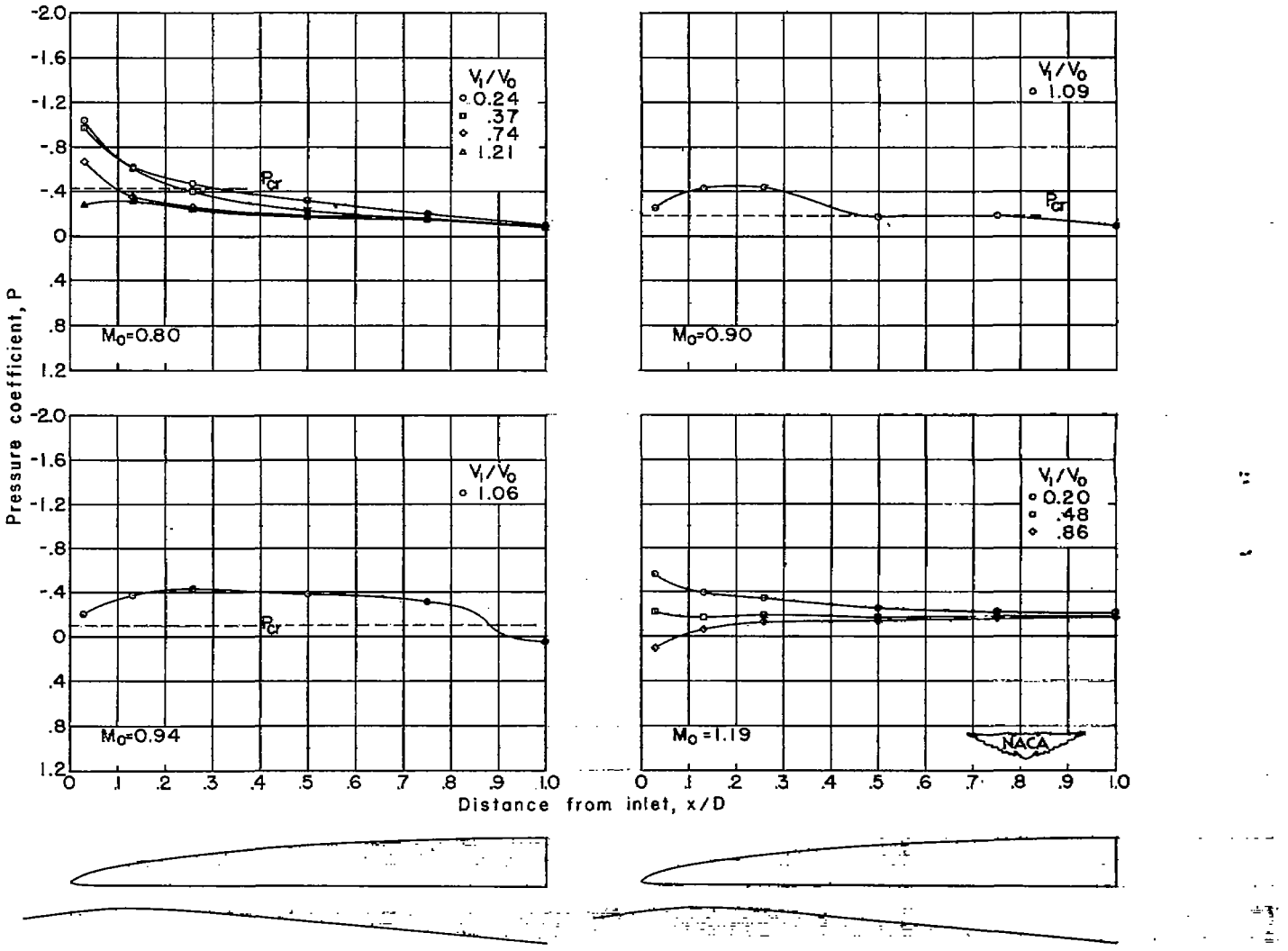

(b) Inlet B.

Figure 11.- Continued.

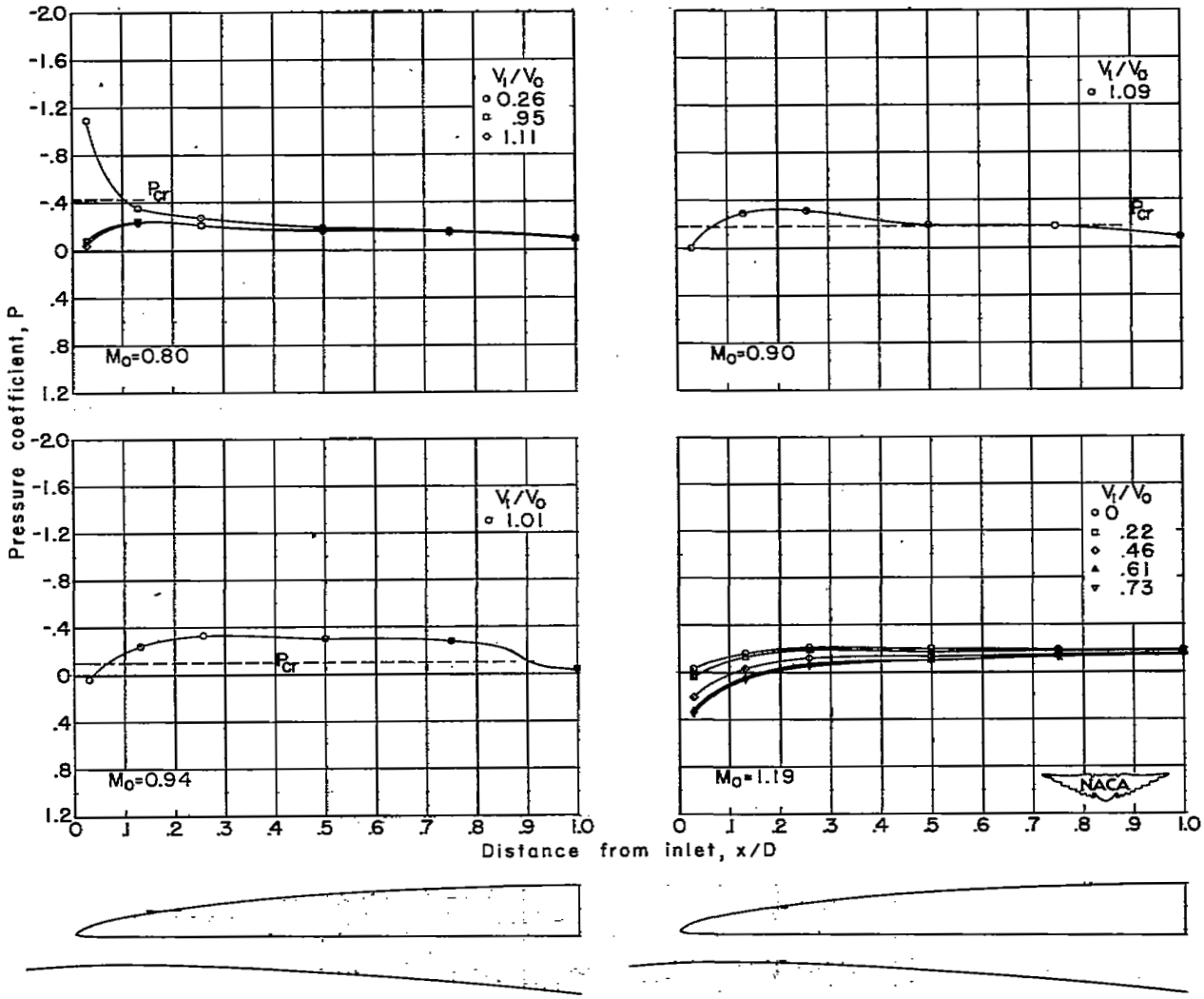

(c) Inlet C.

Figure 11.- Concluded.

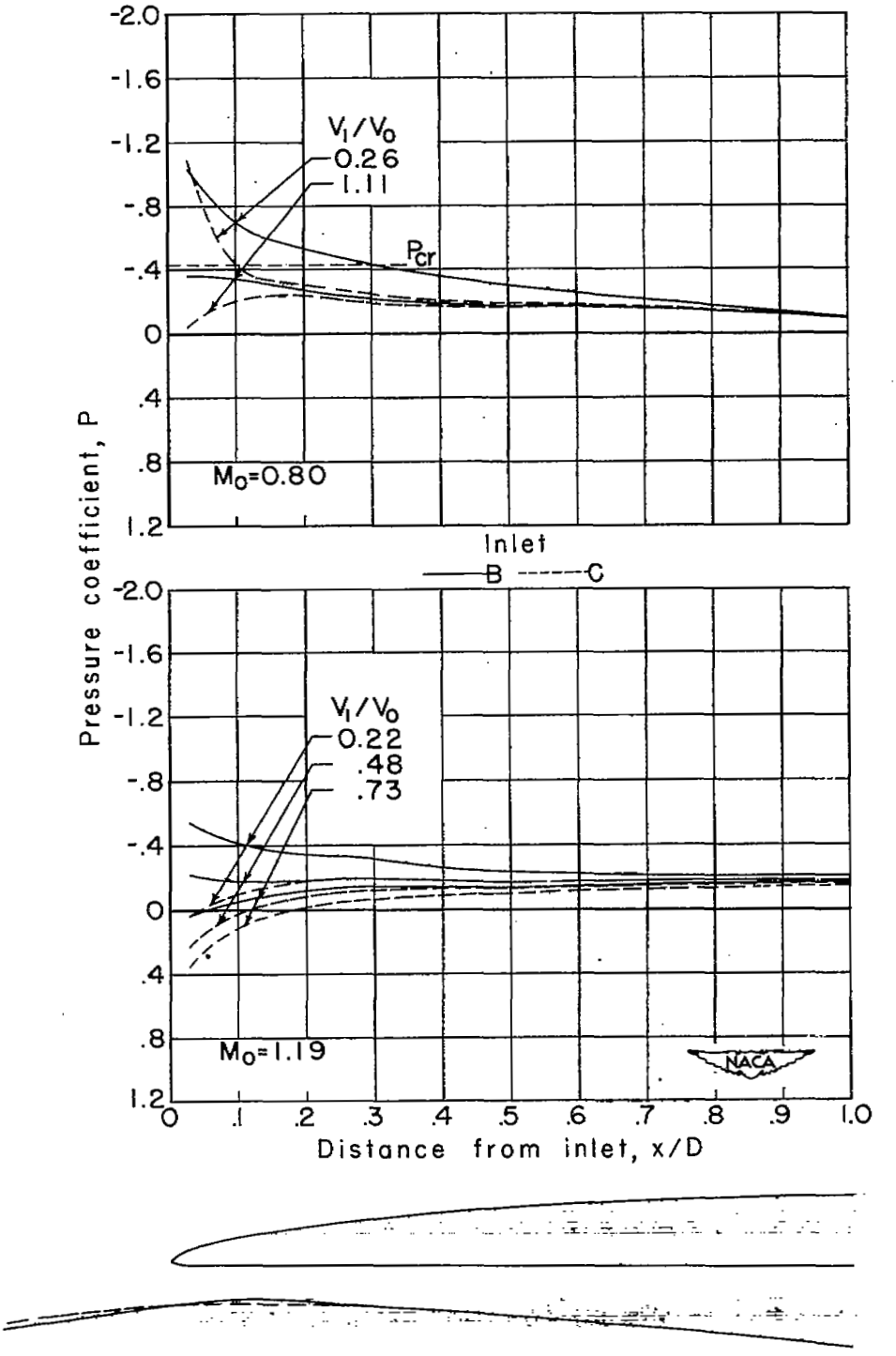

Figure 12.- Effect of central-body shape on external-surface pressure distribution.

[redacted]

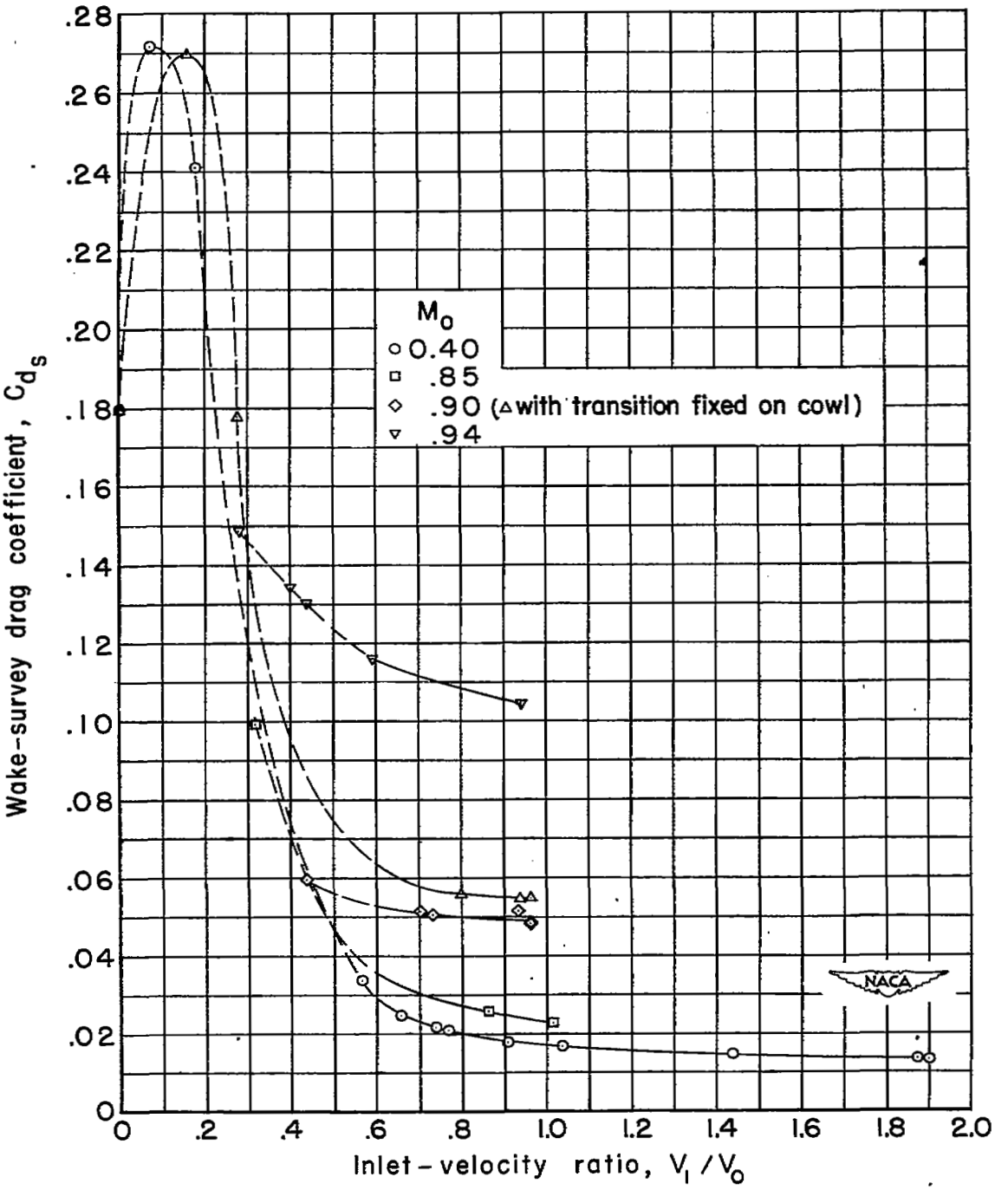

(a) Inlet A.

Figure 13.- Variation of wake-survey drag coefficient with inlet-velocity ratio.

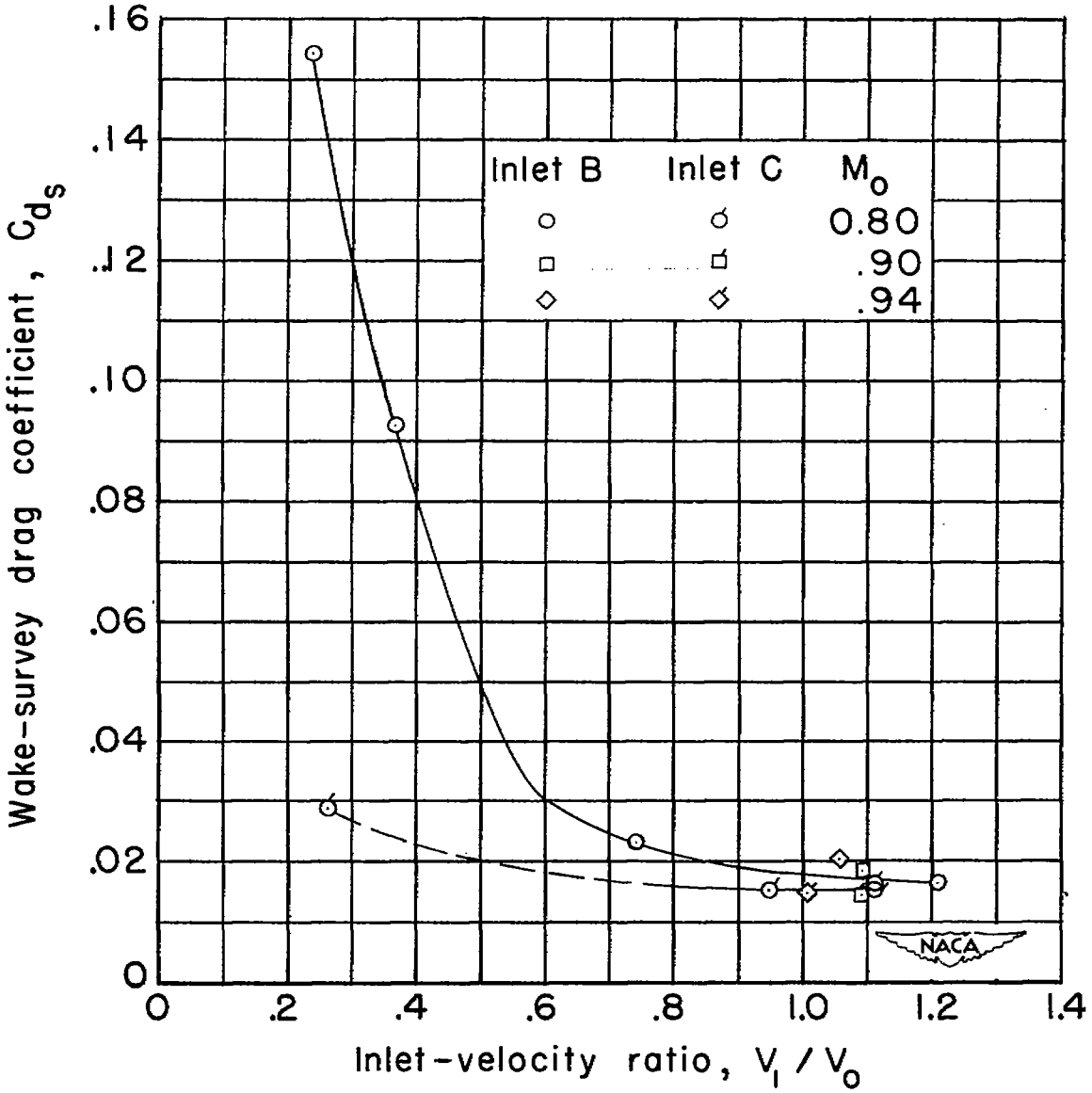

(b) Inlets B and C.

Figure 13.- Concluded.

[redacted]

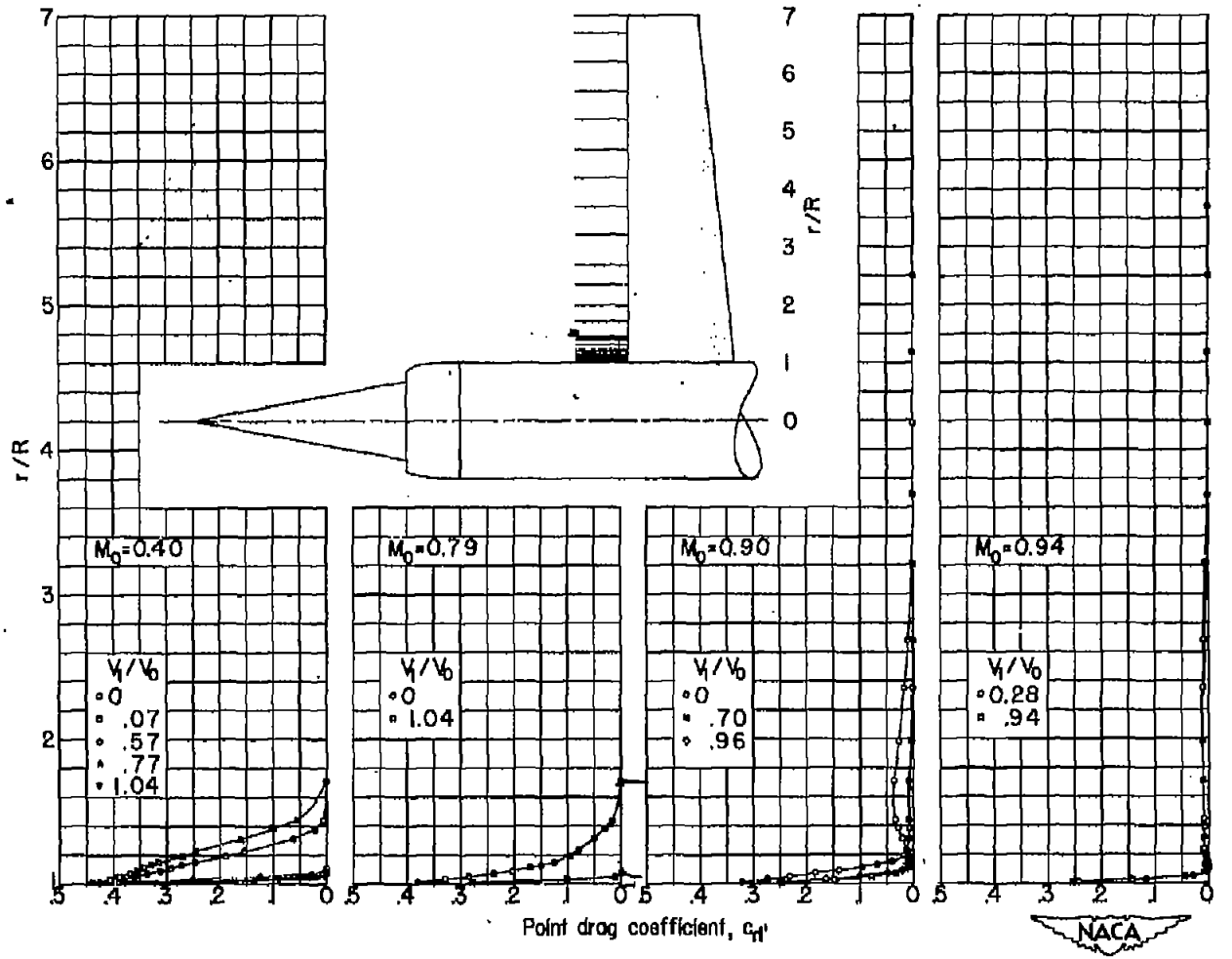

(a) Inlet A.

Figure 14.- Radial distribution of point drag coefficient.

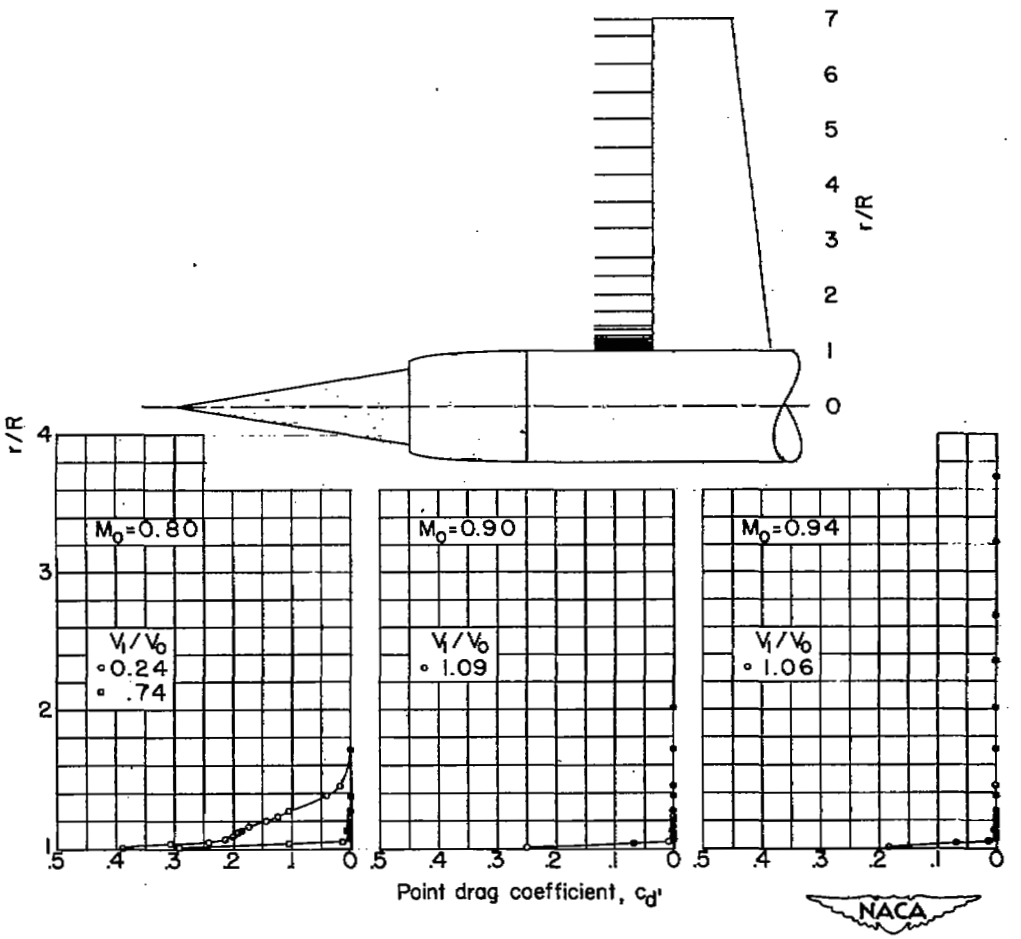

(b) Inlet B.

Figure 14.- Continued.

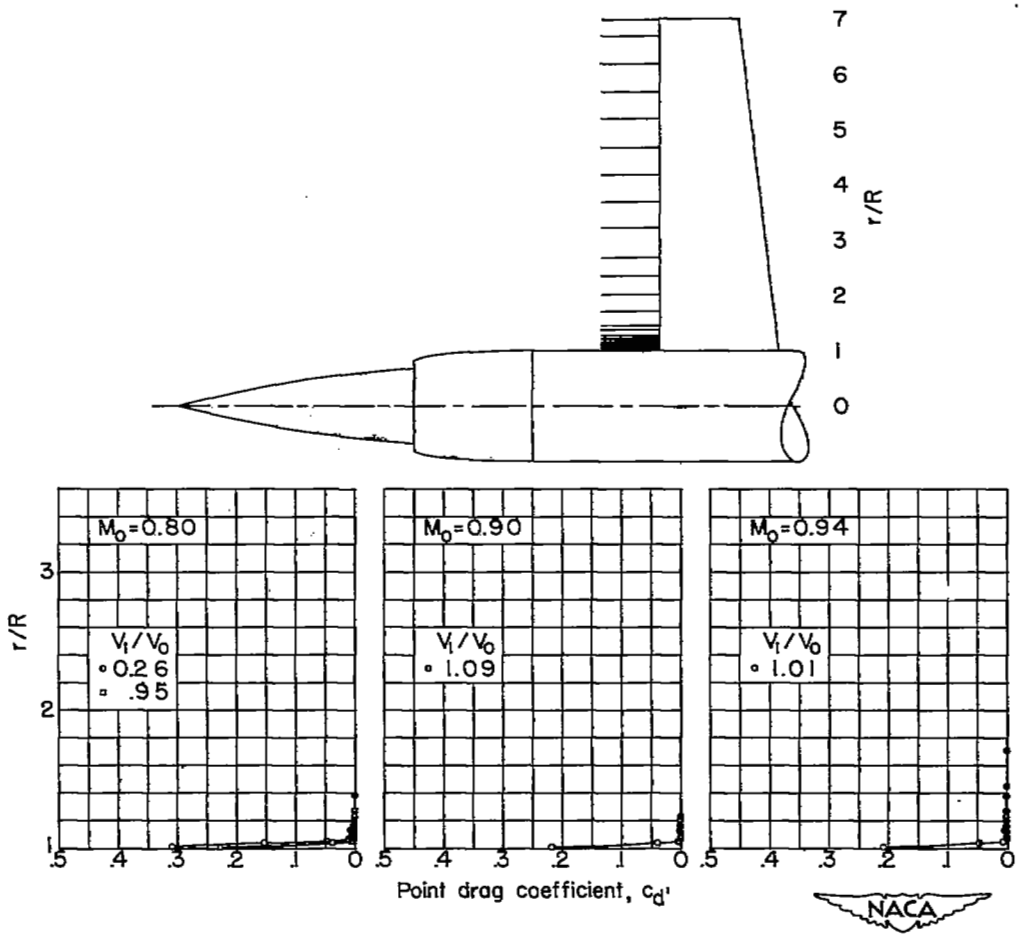

(c) Inlet C.

Figure 14.- Concluded.

[redacted]

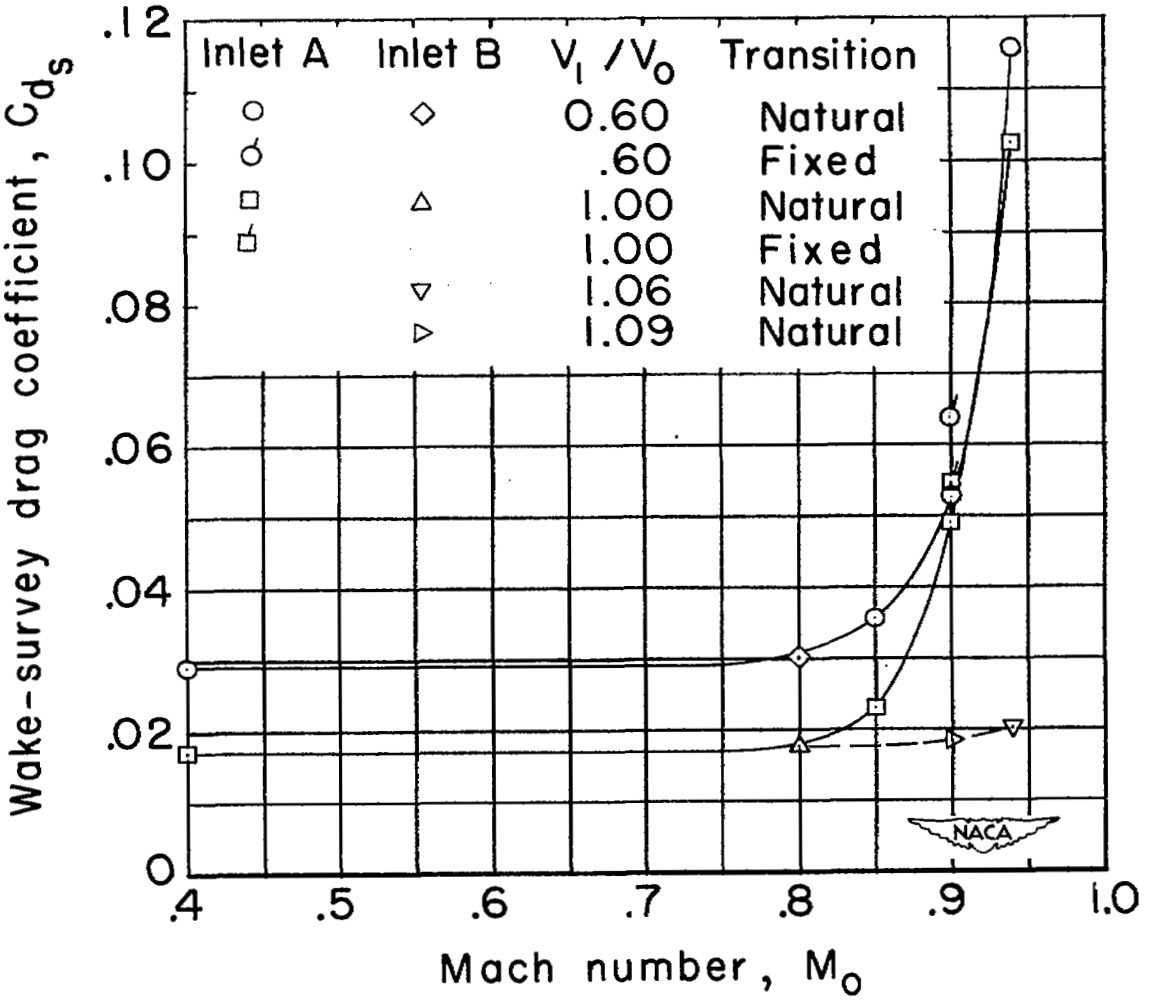

Figure 15.- Variation of wake-survey drag coefficient with Mach number.

[redacted]

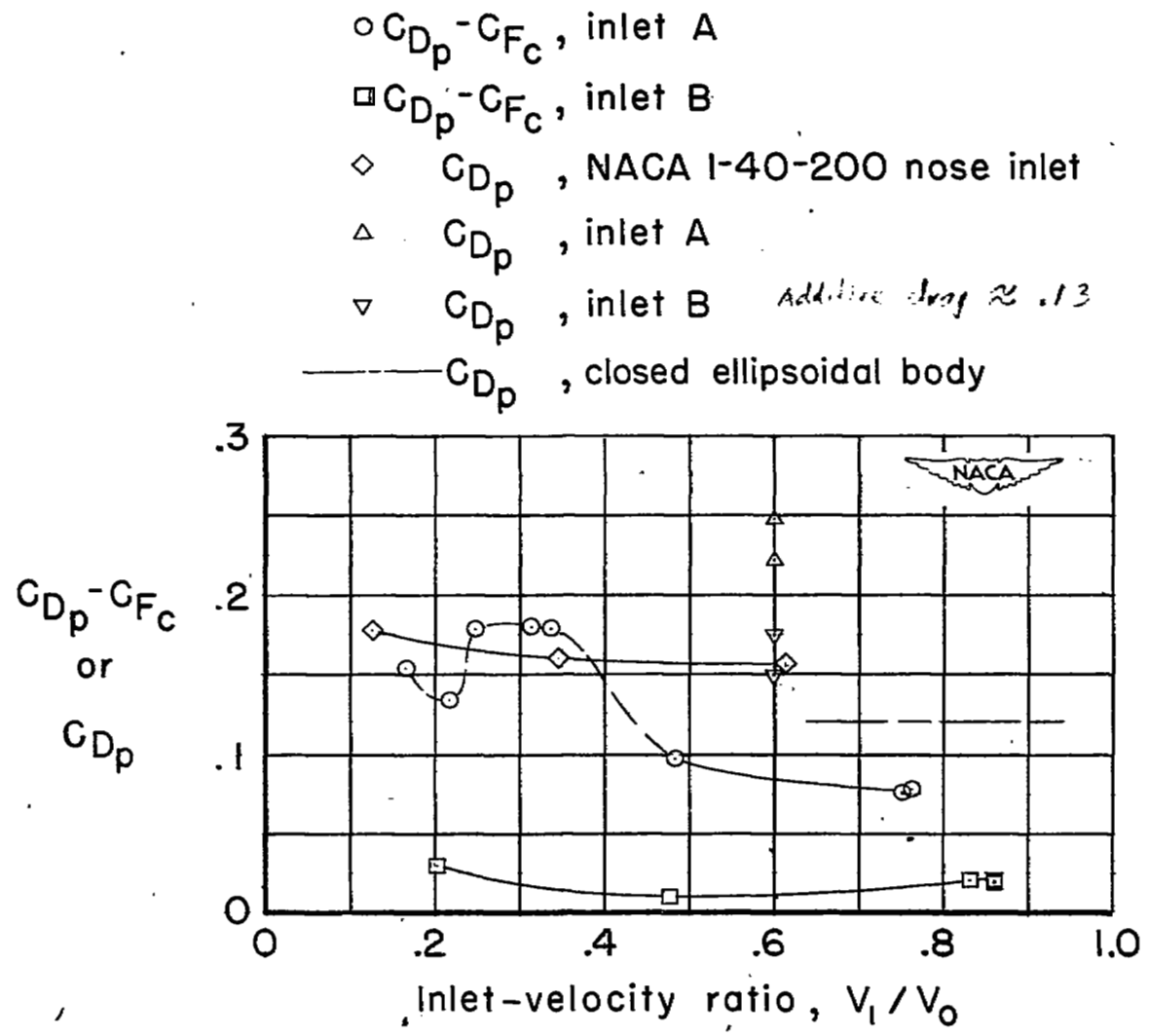

Figure 16.- External pressure-drag comparisons. $M_o \approx 1.2$.